Research Department

Technical Report No. 64

Impact of changes to the radiation scheme in the ECMWF model

by

J-J Morcrette

November 1989

Abstract

A new radiation package, shown to correct most of the systematic errors of the operational ECMWF radiation scheme, has been extensively tested in the ECMWF forecast model. Improvements in the clear-sky fluxes and radiative heating/cooling rate profiles stem mainly from a better representation of the transmission functions. New cloud optical properties have been set from detailed narrow-band calculations providing more realistic models for clouds.

Results indicate a greater overall sensitivity of the model to cloud-radiation interactions. Radiative cooling in the subtropics is increased. A decreased radiative cooling in the higher layers of the tropics is caused by larger longwave impact of the high level clouds. An increase in the radiative energy available at the surface and an overall cooling of the troposphere generate larger turbulent heat fluxes. All these changes contribute to a higher level of convective activity, resulting in a more energetic hydrological cycle and a more active model with higher levels of zonal and eddy available potential and of eddy kinetic energy at all wave numbers. The increased contrast in the disposition of radiative energy between land and ocean, as well as between clear-sky and cloudy areas, improves the distribution of diabatic heating. The warm bias in stratospheric temperature is greatly reduced. The divergence in the tropics is larger and does not weaken as much after a few days of integration as with the old operational radiation scheme, thus improving the Hadley circulation. The radiation budget at the top of the atmosphere is now in good agreement with satellite observations. Several other systematic errors of the ECMWF model are also, partially, corrected.

1. INTRODUCTION

For the last ten years, the European Centre for Medium-range Weather Forecasts (ECMWF) has carried out operational assimilations of meteorological data and has issued 10-day forecasts. From the beginning, forecast errors have been consistently monitored, and a number of papers (Hollingsworth et al., 1980; Heckley, 1985; Arpe and Klinker, 1986; Tiedtke et al, 1988; Arpe, 1988) have focused on the systematic errors in the ECMWF analysis-forecast system and their evolution over the years in relation to the introduction of various changes and improvements in the system.

In a recent paper, Arpe (1988) analysed the errors present in the current system (as from 1 January 1988). They can be separated into three categories with regard to their relationships to potential deficiencies in the radiative transfer parametrization used in the model. Firstly, those which clearly display the signature of a deficient cloud-radiation parametrization, such as the unrealistic smooth field of outgoing longwave radiation at the top of the atmosphere, the stratospheric warm temperature bias and the too small clear-sky radiative cooling in the tropics. Secondly, those which are probably related to an improper three-dimensional distribution of the radiative forcing. In this regard we can note the presence of a negative bias in surface temperature at high latitudes in spring, the slowing down of the model hydrological cycle after 4 forecast days, and the small value of the maximum of the tropical divergence in the troposphere (600-300 hPa). Finally, the third category includes the systematic errors that cannot be connected to weaknesses in the representation of cloud-radiation interactions, such as a poleward and upward shift of the subtropical jets and excessive easterlies in the upper tropical troposphere. The latter two errors are typical of most large-scale numerical models of the atmosphere.

Recently, the Intercomparison of Radiation Codes in Climate Models (ICRCCM) programme (Luther et al., 1988) has provided the opportunity to use the results of very detailed radiation models. They can be considered as state-of-the-art reference calculations, at least in a relative sense, for the much cruder parametrizations used in large-scale numerical models of the atmosphere. Such comparisons have been carried out for the ECMWF operational radiation scheme. They have shown the presence of a number of systematic errors, both in the longwave and shortwave radiation transfer parametrizations, in clear-sky as well as in cloudy atmospheres (Morcrette, 1989).

This paper reports results of an extensive study of the effects of a new radiation scheme which corrects many of the deficiencies of the previous operational radiation code. Section 2 presents the methodology of the experimentation. It gives a short presentation of the new radiation code, including some comparisons of the results of the new and old radiation codes with more detailed radiation models. Detailed results of the comparisons are presented in

section 3 with emphasis on the long-term response of the model. The impact of the change of the radiation scheme on the ECMWF forecast model and its systematic errors is then discussed in section 4.

2. METHODOLOGY

In the following sections, comparisons are presented of two sets of experiments, hereafter referred to as OPE and NEW, respectively. The first includes the control integrations performed with the operational ECMWF forecast model (until the end of April 1989). The second set consists of integrations performed with the same model, but with the new radiation scheme.

A general description of the ECMWF analysis/forecasting system is given by Hollingsworth et al. (1985), the analysis scheme is described in Lönnberg et al. (1986) and Shaw et al. (1987), whereas a more detailed discussion of either the dynamical or the parametrization aspects of the model can be found in Simmons et al. (1988) and Tiedtke et al. (1979, 1988), respectively.

2.1 Experiments

In the following, results from the long integrations at lower horizontal resolution (3 pairs of T42 90-day integrations and 2 pairs of T63 30-day integrations) are used to describe the long-term impact of the new radiation scheme on the "climate" of the ECMWF model, whereas results from the 10-day forecasts (19 pairs of T63 and 12 pairs of T106 10-day integrations) are used to assess the impact on the quality of the forecasts. The initial data for these integrations are spread evenly over the seasons between 1987 and 1988.

2.2 The radiation schemes

The main features of the two radiation schemes are presented in Table 1. The operational scheme (OPE) was originally described in Geleyn and Hollingsworth (1979). The longwave parametrization underwent some revision at the end of 1984, which is discussed in Ritter (1984), and Slingo et al. (1988).

Recently, an extensive validation of OPE was carried out partly through comparisons with detailed models made available through the ICRCCM programme, partly through comparisons of model-generated radiation fields at the top of the atmosphere with well calibrated radiances measured by the Earth Radiation Budget Experiment (ERBE) (Morcrette and Fouquart, 1988). It has shown the presence of a number of systematic errors of which the new radiation scheme is almost free (Morcrette, 1989).

For a clear-sky column, OPE overestimates the shortwave heating by 15-20 percent and underestimates the longwave cooling by 10-15 percent. These systematic differences can correspond to local differences as high as 0.50 K/day in the shortwave and 0.70 K/day in the longwave in layers generally several hundreds of hPa thick, and to a systematic deficit

Table 1a: Summary of the ECMWF operational radiation code (OPE)

Two-stream formulation is employed together with photon path distribution method. The radiative transfer equation is solved first for all processes except gas absorption which is included afterwards.

Ref: Geleyn and Hollingsworth, 1979

a. Clear-sky

(i) Shortwave: Two spectral intervals (0.245-0.78 and 0.78-4.63 7 μm)

Rayleigh scattering	Included
Aerosol scattering and absorption	Possibility of 5 types of aerosols based on climatological models.
H_2O	1 interval
O_3	1 interval

(ii) Longwave: Scattering is neglected. Two-stream method with fast-exponential sum fitting of the transmission functions. Pressure and temperature dependence of absorption is introduced via a one-parameter scaling approximation. Absorption coefficients fitted from AFGL 1980 (Rothman, 1981).

Ref: Ritter, 1984; Slingo et al., 1988

H_2O	5 spectral intervals, only p-type continuum absorption
CO_2	Overlap with H_2O in 2 intervals by multiplication of transmission
0_3	Overlap with H_2O in 1 interval
Aerosols	as in (a.i).

b. Cloudy sky

(i) Shortwave

Droplet absorption and scattering	Treated explicity via the two-stream method with τ and ω defined in terms of LWP (g is preset)
Gas absorption	Included separately through the photon path distribution method.

(ii) Longwave

Droplet absorption and scattering	as in (b.i)
Gas absorption	as in (a.ii)

Table 1b: Summary of the ECMWF new radiation code (NEW)

a. Clear-sky

(i) Shortwave: Two stream formulation employed together with photon path distribution method (Fouquart and Bonnel, 1980) in 2 spectral intervals (0.25-0.68 and 0.68-4.0 μm).

Rayleigh scattering	Parametric expression of the Rayleigh optical thickness
Aerosol scattering and absorption	Mie parameters for 5 types of aerosols based on climatological models (WMO-ISCU, 1984).
Gas absorption	from AGCL 1982 compilation of line parameters (Rothman et al., 1983).
H_2O	1 interval
Uniformly mixed gases	1 interval
O_3	2 intervals

(ii) Longwave: Broad band flux emissivity method with 6 intervals covering the spectrum between 0 and 2620 cm^{-1}. Temperature and pressure dependence of absorption following Morcrette et al. (1986). Absorption coefficients fitted from AFGL 1982.

H_2O	6 spectral intervals, e- and p-type continuum absorption included between 350 and 1250 cm^{-1}
CO_2	Overlap between 500 and 1250 cm^{-1} in 3 intervals by multiplication of transmission
0_3	Overlap between 970 and 1110 cm^{-1}
Aerosols	Absorption effects using an emissivity formulation.

b. Cloudy sky

(i) Shortwave

Droplet absorption and scattering	Employs a delta-Eddington method with τ and ω determined from LWP, and preset g and r_e
Gas absorption	Included separately through the photon path distribution method.

(ii) Longwave

Scattering	Neglected
Droplet absorption	From LWP using an emissivity formulation
Gas absorption	as in (a.ii)

Timing: 98 percent of the operatinal scheme for a 19-level model.

in radiative energy at the surface as large as 50 Wm^{-2}. Similar comparisons for cloudy atmospheres have shown that the reference model cloud originally used to derive the optical properties of the ECMWF model clouds is very different from the mean cloud actually found in the atmosphere. This leads to very large cloud albedoes for realistic cloud liquid water contents (LWCs). To overcome this flaw, clouds are ascribed unrealistically small LWCs, which make the higher level clouds almost radiatively inactive. Such a systematic deficiency also appears in comparisons with satellite observations, and explain together with the deficiencies in the clear-sky parametrization the rather flat field of outgoing longwave radiation at the top of the atmosphere in the model.

The new radiation package (NEW), which includes major changes in both shortwave and longwave radiation parametrizations and in the cloud optical properties, is based on an updated/revised version of the radiation schemes originally developed at the University of Lille (Fouquart and Bonnel, 1980; Morcrette and Fouquart, 1986; Morcrette et al., 1986).

Clear-sky longwave fluxes are evaluated with an emissivity method incorporating a parametrization which provides an improved representation of the temperature and pressure dependence of the absorption processes to the radiative transfer. Scattering is treated with a Delta-Eddington approximation. Transmission functions are developed as Padé approximants. Coefficients for the molecular absorption are calculated from the 1982 version of the AFGL line parameters compilation (Rothman et al., 1983). Cloud shortwave radiative parameters are the optical thickness τ and single scattering albedo ω linked to the cloud liquid water path (LWP), and a prescribed asymmetry factor g (Fouquart, 1987). These cloud shortwave radiative parameters have been fitted to *in situ* measurements of stratocumulus clouds (Bonnel et al., 1983). A distinction can be made between various cloud types by defining τ and ω as functions not only of the liquid water path in the cloud but also of the effective radius r_e of the cloud particles. r_e is then made a function of height in an empirical attempt to account for varying cloud types from stratiform to cumuliform to cirriform. However these features were not used in the experimentation presented hereafter and all clouds particles in the new radiation scheme were prescribed an effective radius r_e of 15 μm.

The new scheme differs from the operational scheme as a result of:

(i) a smaller shortwave H_2O absorptivity, which reduces the clear-sky shortwave heating and increases the downward solar radiation at the surface;

(ii) an improved temperature and pressure dependence of the longwave absorption, which increases the longwave cooling in mid-troposphere and stratosphere; it corrects the underestimation of the clear-sky outgoing longwave radiation (OLR) at the top of the atmosphere shown by the operational radiation scheme;

(iii) the presence of both the e- and p- type components of the H_2O continuum absorption, which cools the tropical planetary boundary layer (PBL) (only p-type absorption is accounted for in the operational scheme);

(iv) cloud optical properties being derived from a more realistic model cloud; as documented in Morcrette (1989), the operational radiation scheme uses cloud optical properties derived from a model cloud, which is a radiation fog (Zdunkowski et al., 1967) with a fairly narrow drop size distribution around an effective radius of 2.25 μm; such a cloud is quite an efficient scatterer already at small LWPs; therefore relatively small cloud LWPs ensure a reasonable description of the net shortwave radiation at the top of the atmosphere; on the contrary, for small LWPs (such as those corresponding to the higher-level clouds), the longwave emissivity is quite low; this, together with the underestimation of the clear-sky outgoing longwave flux, explains the lack of contrast in OLR produced by OPE;

(v) a diagnostic formulation of the cloud liquid water content which is independent of the model's vertical grid; this usually increases the liquid water content (LWC) of the diagnosed layer clouds in NEW integrations compared to OPE integrations.

Figure 1a presents the clear-sky cooling rate profile in a standard mid-latitude summer atmosphere computed by both the OPE and NEW schemes and the results of the GFDL longwave line-by-line model (kindly provided by Dr. Fels). Similarly, Figure 1b compares the clear-sky heating rate profile in the same atmosphere computed by OPE, NEW and the detailed shortwave narrow-band model of Fouquart and Bonnel (1989). Both figures show the large departures of OPE with respect to the detailed models. They are as large as 0.70 K/day in the longwave, corresponding to a 10-15 percent underestimation of the longwave atmospheric absorption and as large as 0.50 K/day in the shortwave, corresponding to a 15-20 percent overestimation of the shortwave atmospheric absorption. Figure 1 also display a much better agreement of NEW with these "reference" models (maximum errors in longwave and shortwave heating rates are 0.15 and 0.10 K/day respectively corresponding to a better than 5 percent agreement on both longwave and shortwave atmospheric absorptions). Such differences also translate into differences in clear-sky downward fluxes at the surface:

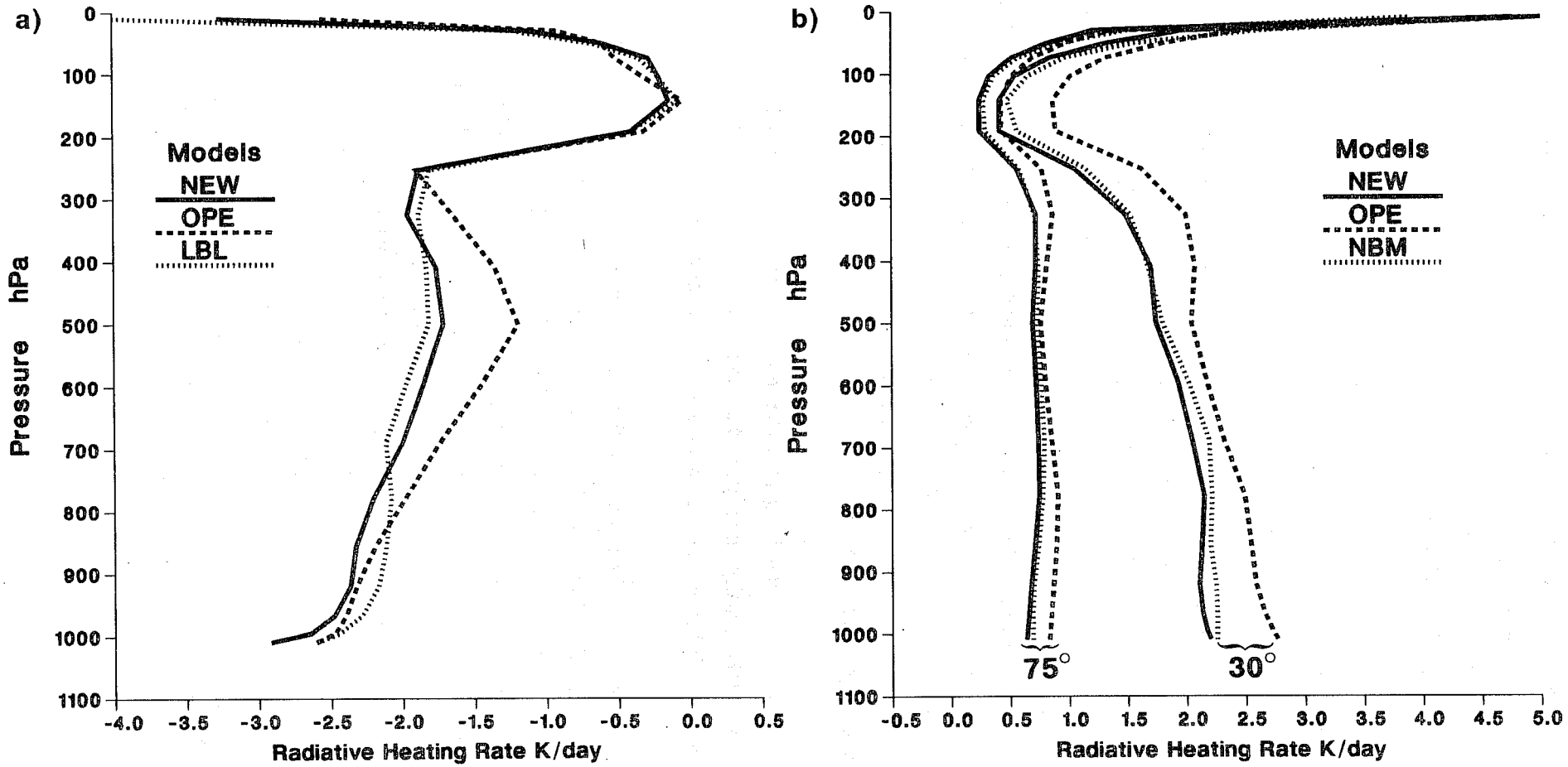

Fig. 1 Comparison of longwave radiative heating rate profiles in a clear-sky standard mid-latitude summer atmosphere. OPE and NEW refer to the operational and new radiation schemes. In the longwave range (Fig. 1a), LBL (dotted line) refer to the results of the GFDL line-by-line model. In the shortwave range (Fig. 1b), NBM (dotted line) refer to the results of the narrow-band model of Fouquart and Bonnel (1988). Shortwave results are presented for a surface albedo A_s = 0.2 and for 2 solar zenith angles, 30° and 75°.

OPE underestimates shortwave fluxes by 3 to 15 percent and longwave fluxes by about 5 percent, whereas fluxes computed with NEW agree within 2 percent with those computed by the detailed models. More extensive comparisons of both the operational and the new radiation schemes with detailed radiation models were carried out for various clear-sky and cloudy standard atmospheres in the framework of the ICRCCM programme. Full results can be found in Morcrette (1989).

The new radiation scheme gives clear-sky fluxes which are in good agreement with detailed radiation models in both the shortwave and longwave parts of the spectrum. The revised cloud optical properties and increased cloud LWC give a much better agreement of the radiation fields produced by NEW with the satellite observations.

3. RESULTS

In this section, results from NEW and OPE integrations of the model are compared with each other and with reference data when available. Most of the fields which are presented to illustrate changes in the ECMWF model's climate, are 30-day averages of the last 30-days of T42 90-day integrations. Moreover, some results are taken from T63 30-day integrations. In the ECMWF model, the systematic errors are very similar at T42 and higher horizontal resolution. It must be stressed that the impact of the change of the radiation scheme, as documented hereafter, is to a first approximation independent of the resolution.

Results from the model integrations are compared with the corresponding ECMWF analyses for all variables available, and various climatologies for diagnosed variables. Although the analyses are known to contain the systematic errors in the ECMWF data assimilation system at the time the analyses were performed, the more recent analyses have been shown to be of better quality (Arpe and Klinker, 1986; Brankovic, 1986; Hollingsworth, 1987). It is therefore consistent to compare results of the last versions of the forecast model to those analyses known to be prone to smaller systematic errors.

3.1 Global budgets

Both the energy and hydrological cycles are affected by the change of radiation scheme. They are intensified by about 20 and 15 percent respectively, as is evident from the global mean values of net radiative cooling and net heating by convection, large-scale condensation and surface heat fluxes (Fig. 2), and from the values of precipitation and surface evaporation (Fig. 3). When compared with the climate estimates of Hoyt (1976), the new radiation scheme produces too high values of the energy balance (NEW: 109 Wm^{-2} ; OPE: 89 Wm^{-2}), with similar results for the hydrological cycle when compared with Jaeger's (1976) climatology. However, the more recent climatology of Verstraete and Dickinson (1986) indicates higher values at 105 Wm^{-2} for the mean annual atmospheric energy budget.

In the early stages of the forecasts, an intense spin-up of the hydrological budget shows up as a large imbalance between the moisture supply by surface evaporation and the loss due to precipitation. The result is that the model dries during the forecast. The new radiation scheme does not improve on this. Furthermore, as all the experiments presented in this paper have been run from initial conditions analysed with the model which included the operational radiation scheme, there is an even larger spin-up in the NEW experiments.

Figure 2 shows that, after the initial adjustment period, the atmospheric energy budget is increased through increase in cumulus convection (by about 25 percent, from 47 to

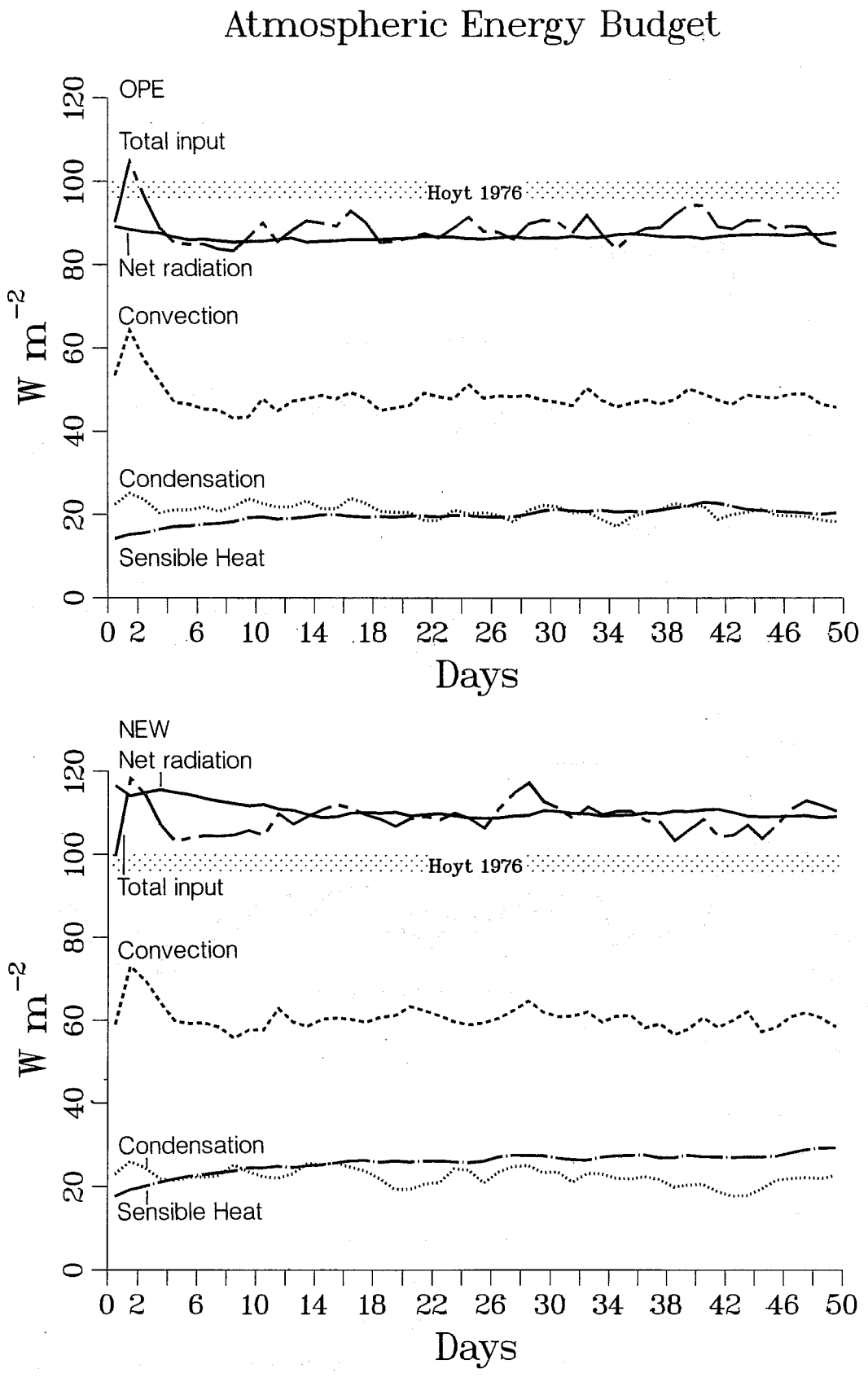

Fig. 2 Time evolution of diabatic heating due to radiation, cumulus convection, large-scale condensation and turbulent heat transfer for the whole globe in operational forecast (top) and forecast with new radiation scheme (bottom). Initial date is 01/06/87.12Z. Results are for the first 50 days of T42 90-day integrations. Climatological data from van Hoyt (1976).

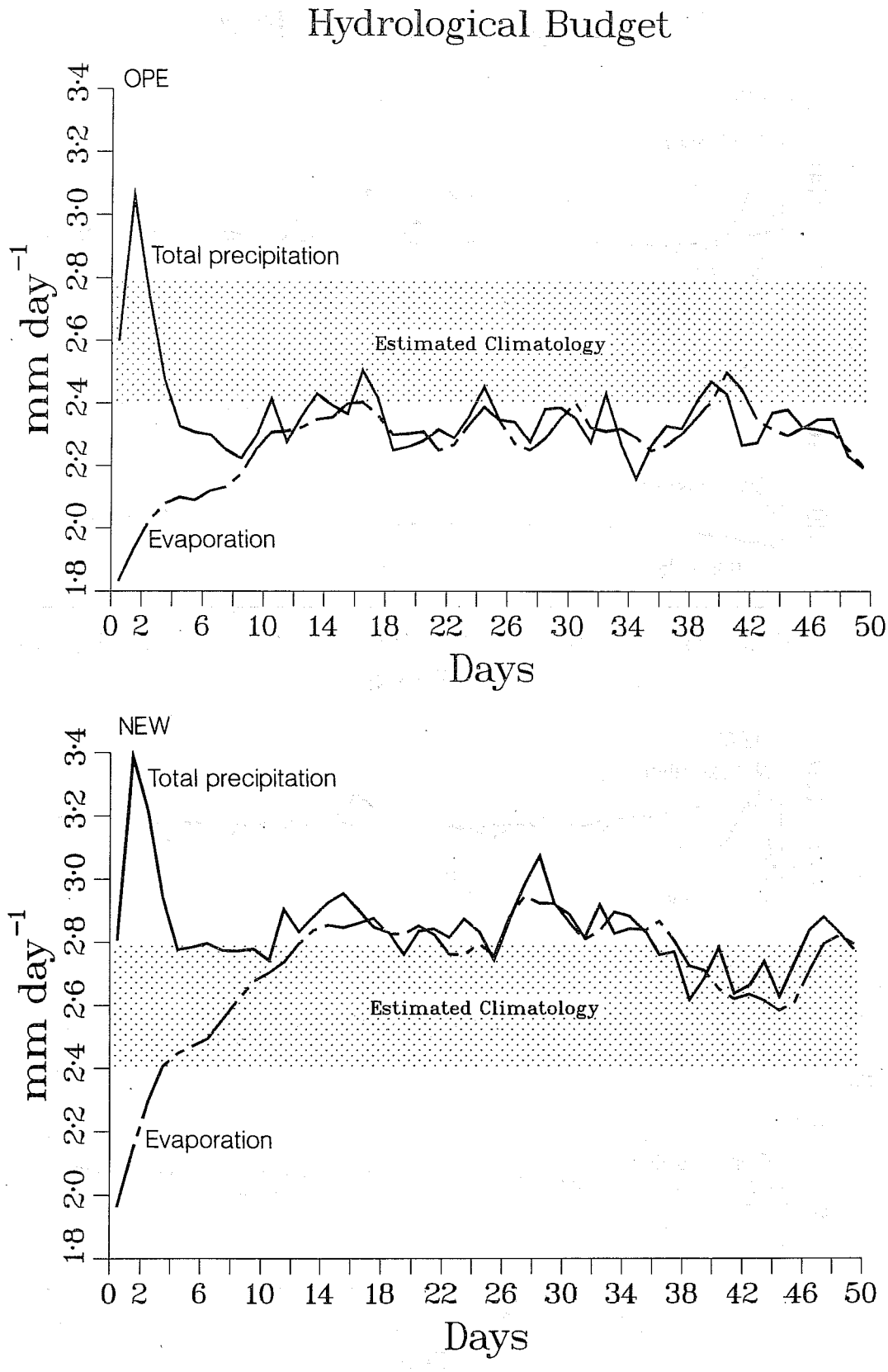

Fig. 3 As in Fig. 2, but for total precipitation and surface evaporation. Climatological data are from Jaeger (1976).

60 Wm^{-2} for the experiments illustrated) and in surface sensible heat (by about 30 percent, from 20 to 26 Wm^{-2}) with a rather constant contribution from large-scale condensation (20 Wm^{-2}). The surface energy budget, shown in Figure 4 is also increased (by about 10 percent, from 162 to 177 Wm^{-2}). The change of radiation scheme gives an increased input of solar radiation (by about 12 percent, from 160 to 180 Wm^{-2}) and a decreased output of terrestrial radiation (by about 10 percent, from 75 to 67 Wm^{-2}). As the model sea surface temperature (SST) is specified, only the land surface can adjust to a larger radiative input. The increased global latent and sensible heat fluxes (by 20 and 30 percent, from 68 to 80 Wm^{-2}, and from 20 to 26 Wm^{-2}, respectively) mainly reflect the cooling of the lower troposphere by NEW.

3.2 Radiation fluxes

3.2.1 At the top of the atmosphere

The new radiation scheme corrects the underestimation of the clear-sky OLR at the top of the atmosphere shown by OPE. Higher cloud LWC and the revised longwave optical properties make the clouds radiatively more active in the longwave part of the spectrum. This leads to increased contrast in OLR fields at the top of the atmosphere (Fig. 5b) with marked minima (< 200 Wm^{-2}) over convective areas and maxima over clear-sky (> 300 Wm^{-2}) or low-cloud-topped areas in agreement with satellite observations. This is an important improvement to the operational scheme (Fig. 5a) which fails to reproduce these features (OLR is in the 230-285 Wm^{-2} range in the tropics). The satellite-derived OLR used as reference (Fig. 5c gives the 30-day mean OLR derived by NOAA Climatic Analysis Center from the operational meteorological satellites) is computed from AVHRR measurements on board operational meteorological satellites through a regression between window radiance measurements and total longwave fluxes. When compared to ERBE data, they tend to show smoothed out features with underestimated high values and overestimated low values, therefore, the NEW model OLR, which displays larger contrast, may even be closer to reality than is shown in Fig. 5.

The shortwave radiation at the top of the atmosphere shown in Fig. 6 is not as drastically modified as the longwave. The operational radiation scheme gives a reasonable contrast between high albedo over cloud areas and low albedo over clear-sky oceans when compared with satellite observations. However, this has been obtained for clouds with relatively small liquid water path (LWP) as discussed in Morcrette (1989), a result linked to the highly reflecting model cloud embedded in the operational scheme and to the small value of the proportionality factor relating the saturation water mixing ratio to the diagnosed cloud liquid water content. The new radiation scheme with its new cloud optical properties and

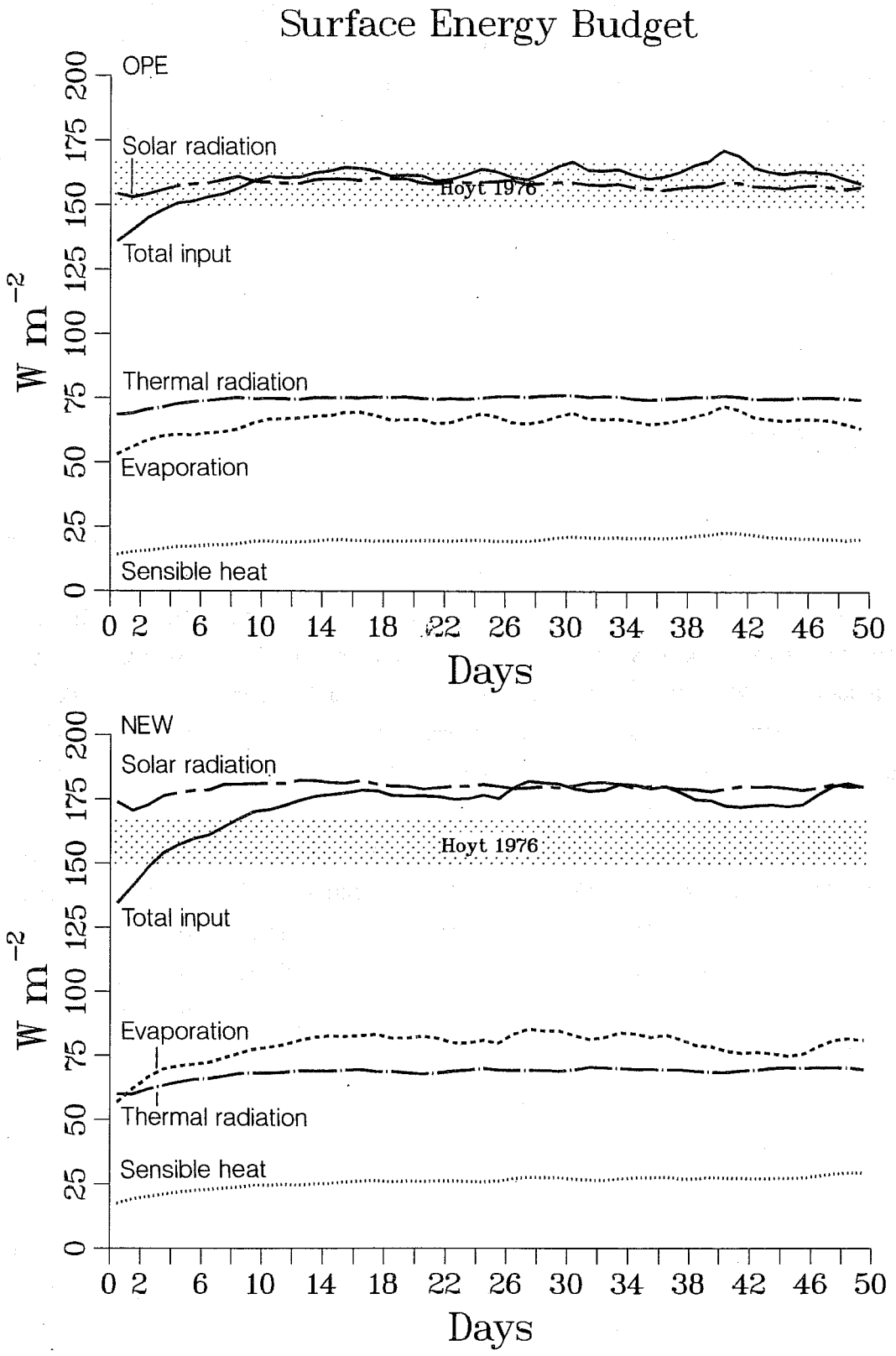

Fig. 4 As in Fig. 2, but for the components of the surface energy budget, namely net solar radiation, net thermal radiation, sensible and latent heat fluxes. Climatological data from van Hoyt (1976).

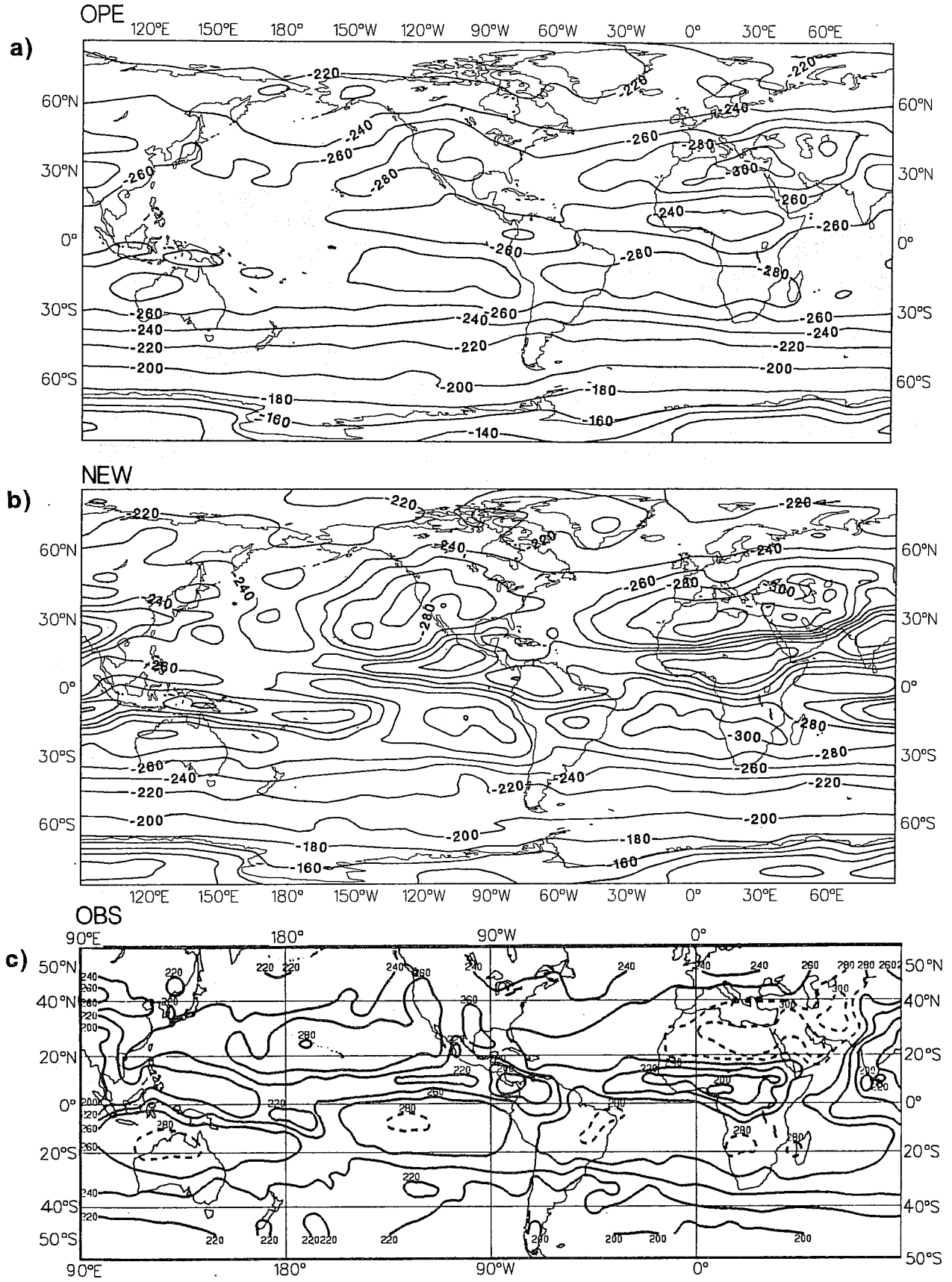

Fig. 5 Outgoing longwave radiation at the top of the atmosphere averaged over the last 30 days of T42 90-day integrations with OPE (top) and NEW (middle). Initial date is 01.06.87,12Z. Bottom figure is the 30-day mean OLR operationally derived by NOAA from AVHRR measurements (NOAA, 1988).

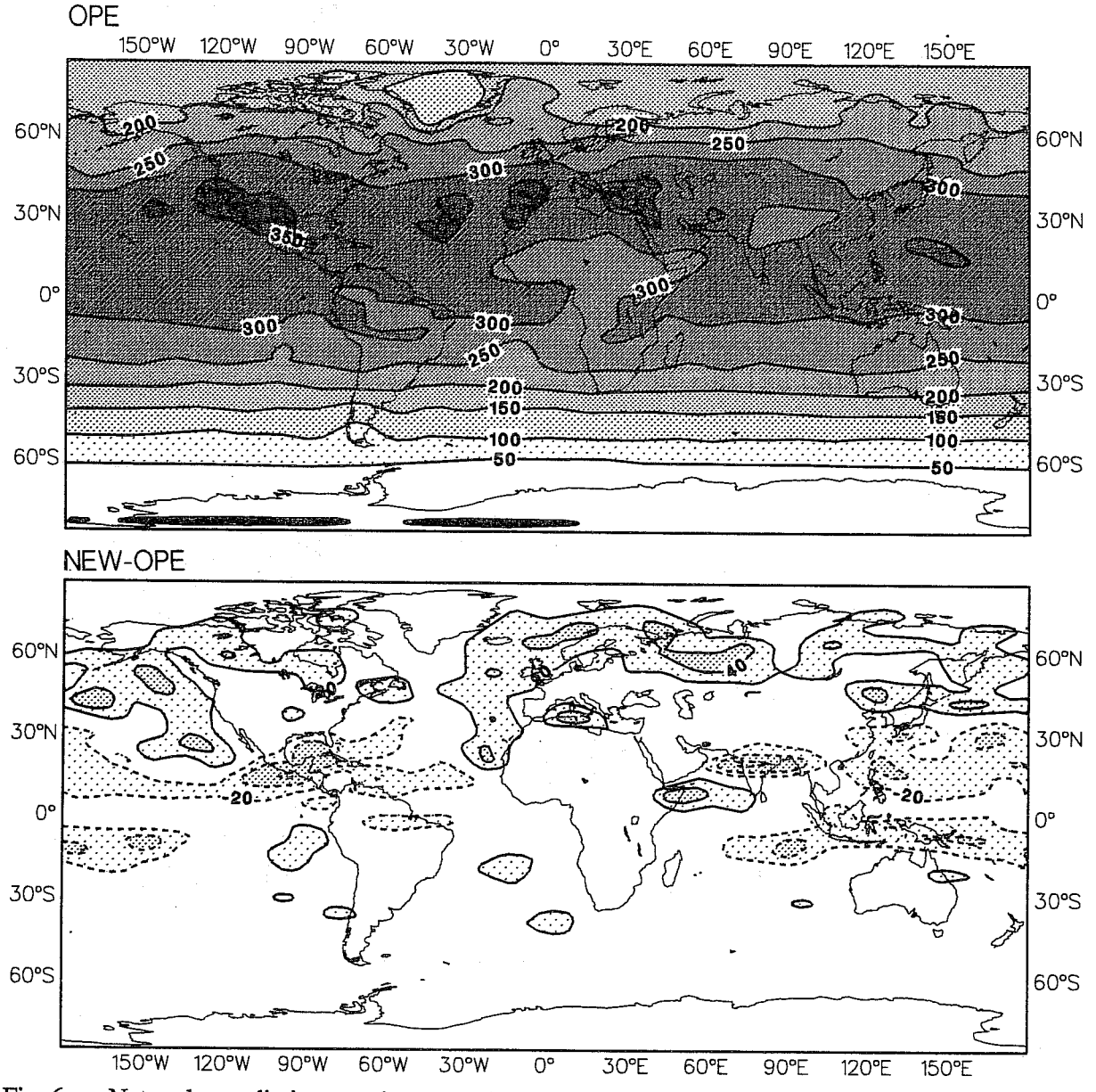

Fig. 6 Net solar radiation at the top of the atmosphere averaged over the last 30 days of T42 90-day integrations with OPE (top: interval is 50 W m^{-2}) and difference NEW-OPE (bottom: interval is 10 W m^{-2}). Initial date is 01.06.87,12Z.

higher LWP gives similar global and zonal means of the shortwave radiation at the top of the atmosphere, but somewhat enhances the longitudinal contrast between clear-sky and cloudy areas.

3.2.2 At the surface

The direct impact of the revised shortwave H_2O absorptivity is to decrease the clear-sky shortwave atmospheric heating. Therefore, more solar radiation is available at the surface as seen in Figure 7. The increased cloud LWP and modified optical properties contribute to increase the shading effect of the clouds thus increasing the contrast in downward shortwave radiation between clear-sky and cloudy areas (about 40 Wm^{-2} less under convective clouds over India and Central America, but about 60 Wm^{-2} more in clear-sky areas in the Indian ocean, or West of California and Mauritania). In the longwave, the new radiation scheme gives larger downward radiation, as a consequence of the better representation of the temperature and pressure dependence of the absorption. In the tropics, this increase is reinforced by the presence of the e-type component of the water vapor continuum as seen in Figure 8. The downward longwave flux also increases in the regions of convective cloudiness. Here again, it leads to more contrast between clear-sky and cloudy areas (see the 150 instead of the 125 Wm^{-2} line over the clear-sky Sahara and Afghanistan and the extent of the 10 Wm^{-2} difference line over most of the tropics in the NEW integration).

These changes in net longwave and shortwave radiation combine and sometimes partially compensate. However, NEW gives larger net radiative fluxes at the surface. North of 60°S, differences between NEW and OPE are in the range 20 to 60 Wm^{-2}.

3.3 Cloudiness

In the ECMWF model, the cloudiness is diagnosed following Slingo (1987). Four types of cloudiness may be present at a time over a given model grid-box, namely three layers of low-, medium-, and high-level clouds each occupying one model layer ("stratiform clouds"), and a convective cloud vertically extending over all layers undergoing convective adjustment. The cloud LWC is set as 1 percent of the mass mixing ratio of saturated water vapor in the layer where the cloud is located. The new radiation scheme uses similar cloud fractions but uses for the "stratiform clouds" the vertically integrated LWP over all clouds diagnosed within the atmospheric slice. This makes the formulation of the cloud LWP independent of the model vertical grid structure and usually gives "stratiform clouds" larger LWP than the operational formulation does.

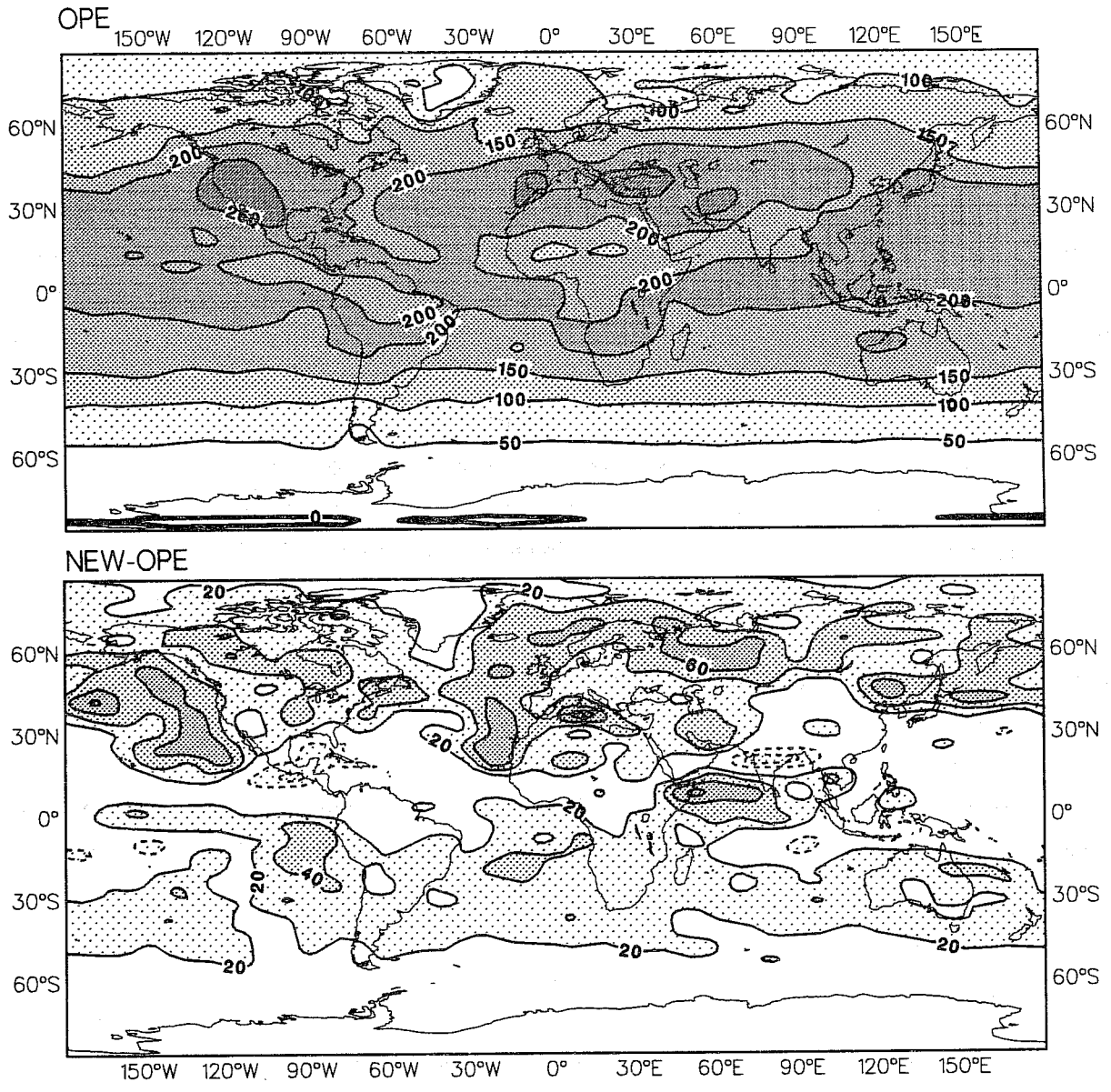

Fig. 7 As in Fig. 6, but for net solar radiation at the surface. Intervals are 50 and 20 W m^{-2}, respectively.

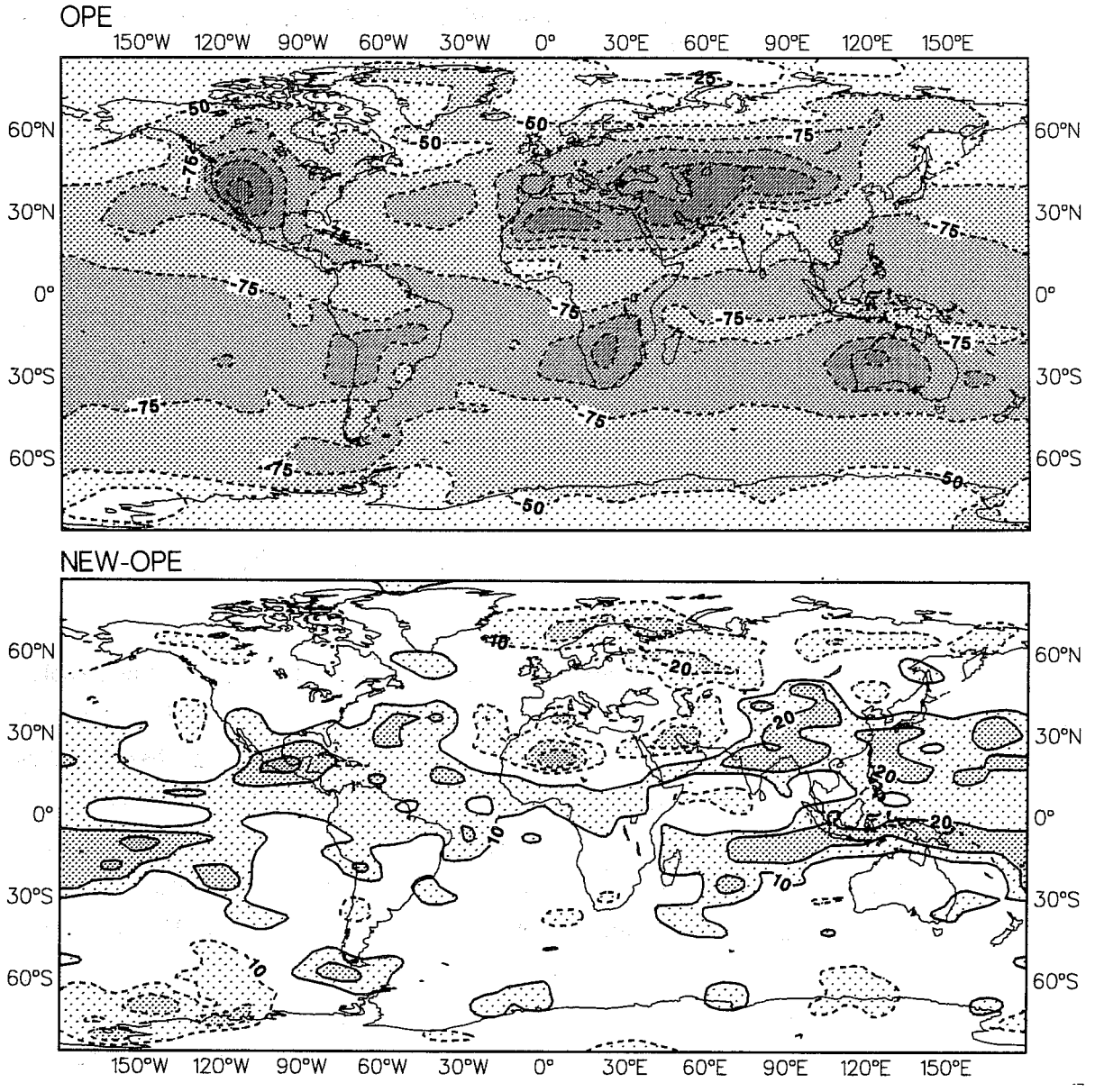

Fig. 8 As in Fig. 6, but for net longwave radiation at the surface. Intervals are 25 and 10 W m^{-2}, respectively.

Table 2

Comparison of cloudiness averaged over the last 30 days of T42 90-day winter and summer integrations. Summer integrations start from 01/06/87.12Z, winter integrations from 01/12/87.12Z. Cloud cover diagnosed following Slingo (1987) includes convective, and high-, medium-, and low-level cloudiness.

	LAND				OCEAN			
	conv.	high	medium	low	conv.	high	medium	low
				SUMMER				
OPE	7.4	25.1	21.4	13.1	10.6	26.2	17.8	16.9
NEW	8.9	26.8	20.0	12.0	11.9	29.1	17.3	17.9
				WINTER				
OPE	5.3	24.2	24.9	24.8	10.3	27.3	16.6	16.3
NEW	6.4	26.1	25.5	24.5	11.7	29.5	17.0	17.2

As can be seen from Fig. 9 for geographical distribution of total cloudiness or from Table 2 which compares the global means of the cloudiness at different levels in the winter and summer T42 90-day integrations, the introduction of the new radiation scheme has an impact on both the vertical and horizontal distributions of the cloud cover. The main features are the increases in convective and high-level cloudiness. For both seasons, the convective cloudiness increases by about 20 and 10 percent over land and ocean, respectively. The high-level cloudiness, which is partly linked to the convective activity in the ECMWF model through the diagnosed anvil cirrus clouds (Slingo, 1987), has this increase in the tropics. Global means of high-level cloudiness increase between 7 and 11 percent depending on season and location. The medium-level cloudiness slightly increases in the winter, but decreases in the summer. The low-level cloudiness decrease over land but increases over the ocean.

These changes in the cloud cover are also partly responsible for the differences seen in the radiation fields (section 3.2): However, the main effect, namely the increased contrast between clear-sky and cloudy areas mainly stems from a better description of the radiation transfer in clear-sky conditions and from changes in the cloud optical properties in the radiation scheme.

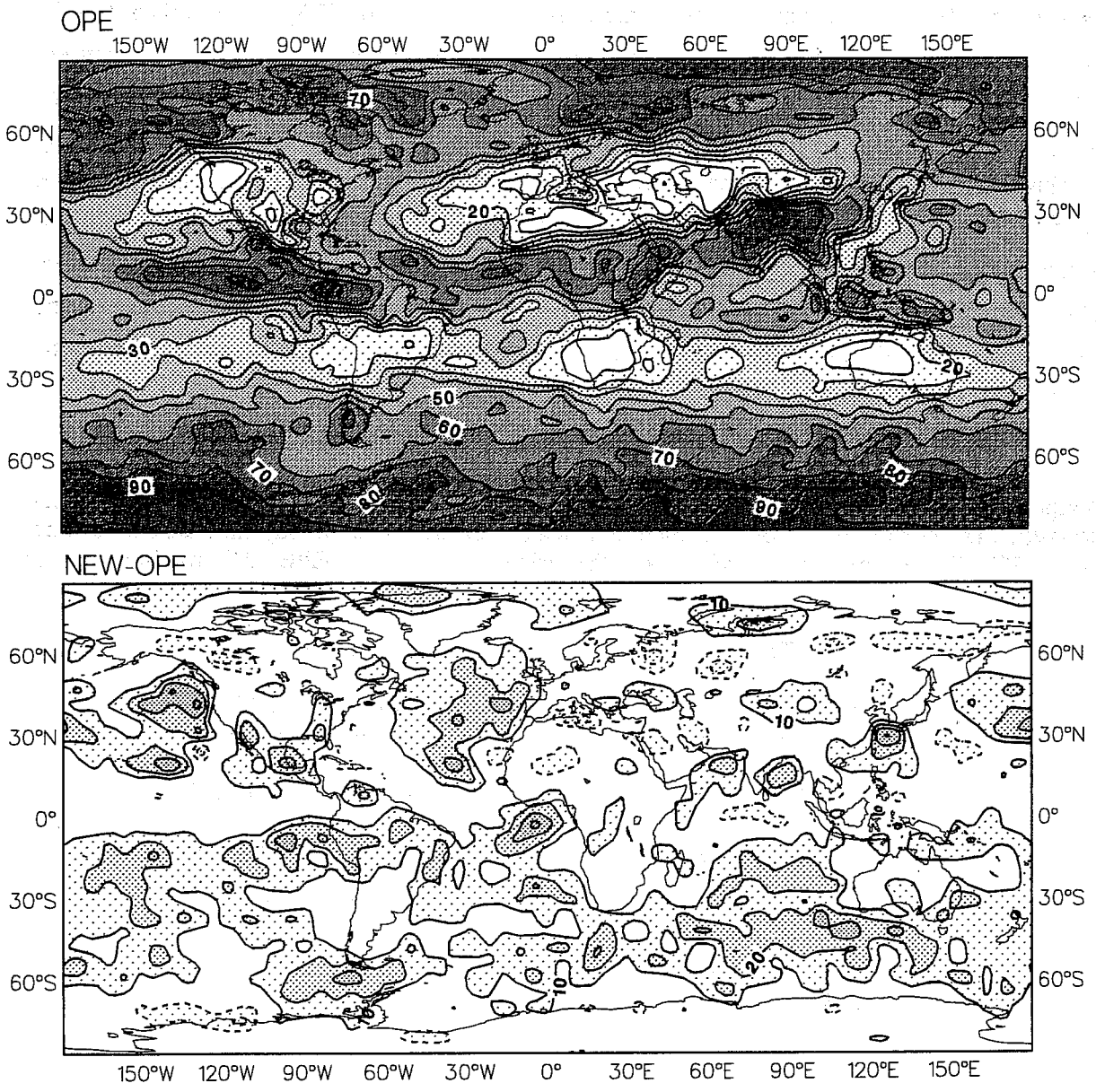

Fig. 9 As in Fig. 6, but for total cloudiness. Intervals are 10 percent on both figures.

The main impact can be seen in the cloud radiative forcing (the difference between the radiative fluxes that would be obtained in absence of cloudiness, all other fields being equal, and the radiative fluxes in presence of cloudiness, following the definition of Ramanathan, 1987). As discussed by Ramanathan (1987) and by Slingo and Slingo (1988), the cloud shortwave forcing (CSF) at the top of the atmosphere is negative everywhere corresponding to a cooling of the atmosphere-surface system by the albedo effect of clouds. The cloud longwave forcing (CLF) at the top of the atmosphere is positive everywhere showing that clouds warm the system by enhancing the greenhouse effect. Apart from cloud reflection, the atmosphere is rather transparent to solar radiation. The CSF has its major impact at the surface. On the contrary, the vertical distribution of the CLF can vary quite substantially depending on latitude, and on the height and emissivity of the cloud. In the experiments reported here, the largest impact of the change of radiation scheme is in the tropics.

Table 3

Components of the radiation budget at the surface and top of the atmosphere over typical clear-sky and cloudy areas of the monsoon region in the T42 90-day integrations starting 1/06/87.12Z. Figures between brackets are the values obtained by OPE. All quantities are in Wm^{-2}.

	CLEAR		CLOUDY	
	LW	SW	LW	SW
Top	305 (275)	360 (345)	165 (225)	255 (275)
Surface	85 (95)	290 (230)	25 (45)	150 (175)
Diverg.	220 (180)	70 (115)	140 (180)	105 (100)

Difference clear-cloudy

	LW	SW	NET
Top	140 (50)	-105 (-70)	35 (-20)
Surface	60 (50)	-140 (-55)	-80 (-5)
Atmosphere	80 (0)	35 (-15)	115 (-15)

Table 3 compares the radiation components at the surface and top of the atmosphere for two neighbouring areas within the monsoon region in summer, one clear-sky area located at the tip of India (5°N, 85°E) and one area where deep convective clouds are well established during most of the last 30 days of the 90-day experiments (27°N, 89°E). While this simple comparison does not provide actual cloud forcing in a "clean" way as proposed by Ramanathan (1987), it gives some hints on the way the new radiation scheme modifies the

cloud contribution to the radiative heating in the core of the tropics. Apart from the increased contrast between clear-sky and cloudy areas already noted in previous sections, NEW gives a completely different picture of the surface-cloud-radiative interactions. Each term in the budget is larger with NEW and the resulting atmospheric balance is of opposite sign. Where the deep clouds in OPE have a small cooling effect on both the atmosphere and the surface (-15 and -5 Wm^{-2}, respectively), they contribute to a substantial heating of the atmosphere (+115 Wm^{-2}, i.e., about 0.95 K/day) and a cooling of the surface (-80 Wm^{-2}) in NEW. Moreover, the larger individual longwave and shortwave terms also show that the diurnal modulation of both the atmospheric and surface energy balance will be larger. Finally the amplitude of the longwave effect of the cloud is such that it cannot be neglected compared to the latent heat released by convection, as already stated by Ramanathan (1987) and Slingo and Slingo (1988), especially if we consider that the cloud heating may be concentrated in the middle to high troposphere.

3.4 Other surface fields

The enhancement of the radiative energy available at the surface can modify the energy and moisture balance of the surface. In our model where sea surface temperature is specifed, this additional radiative energy may contribute to a heating of the land surface or/and return to the atmosphere as increased turbulent fluxes over land. The actual conversion strongly depends on the season, the latitude, the moisture content of the surface. Over the ocean, any change in turbulent heat fluxes reflects a change in the temperature and/or humidity of the lowest tropospheric layer.

Table 4 compares the radiative and turbulent heat fluxes and related surface temperature and moisture obtained for both sets of T42 90-day summer and winter integrations. The increase in radiative energy available at the surface mainly leads to an increase in both sensible and latent heat fluxes (SH and LH, respectively), with larger increases of SH over land and of LH over the ocean, mainly due to a cooler lower troposphere (see 3.6). For example, in the summer integration, one can observe an increase of the sensible heat flux over most of the continents (Fig. 10) and an increase of the latent heat flux over most of the subtropical oceans (Fig. 11). The impact on surface temperatures is smaller and on soil moisture is of secondary importance. In winter, the increase in radiative energy contributes to higher surface temperatures at higher latitudes over North America and Eurasia (by 1 to 2 K).

The validation of these features is difficult due to the absence of corresponding climatological values over the continents. Verstraete and Dickinson (1986) give mean annual values for SH and LH over land of at 31 and 36 Wm^{-2}, respectively, corresponding to a mean Bowen ratio of 0.86. Bowen ratios for the ECMWF model are higher (0.94 and 1.06 for OPE and NEW, respectively, with seasonal variations of up to 20 percent around those

values). Over the ocean, the latest climatological estimates of the components of the surface energy budget are those of Esbensen and Kushnir (1981). With reference to those, OPE gives high estimates of the surface shortwave and longwave radiation and of the sensible heat flux; NEW gives even higher estimates of the shortwave radiation and sensible heat flux but longwave radiation is in better agreement; the climatological latent heat flux estimates of Esbensen and Kushnir are between those by OPE and NEW. However, it must be pointed out that the uncertainties in these climatological estimates are quite large. For example, Arpe and Esbensen (1988), using the more recent climatology of latent heat fluxes compiled by Oberhuber (1988), have recently pointed out the underestimation of the latent heat flux by the ECMWF operational model in the subtropics. Results of the NEW integrations are in that respect in better agreement with this more recent climatology.

Table 4

Comparison of surface fields averaged over the last 30 days of T42 90-day winter and summer integrations. Summer integrations start from 01/06/87.12Z, winter integrations from 01/12/87.12Z.

	LAND						OCEAN			
	SH	LH	LW	SW	Ts	Ws	SH	LH	LW	SW
					SUMMER					
OPE	44.6	40.3	80.7	174	13.6	0.93	12.3	77.9	69.6	148
NEW	58.3	48.9	78.3	196	14.7	0.92	15.0	91.4	61.3	166
					WINTER					
OPE	22.5	29.5	70.1	121	1.0	1.07	14.5	79.2	71.2	181
NEW	31.1	33.7	68.1	134	1.7	1.07	17.9	92.9	63.5	204

SH: Sensible heat flux (Wm^{-2}) ; LH: Latent heat flux (Wm^{-2})

LW: net upward longwave radiation (Wm^{-2})

SW: net downward shortwave radiation (Wm^{-2})

Ts: surface temperature (Celsius) ; Ws: Soil moisture (mm)

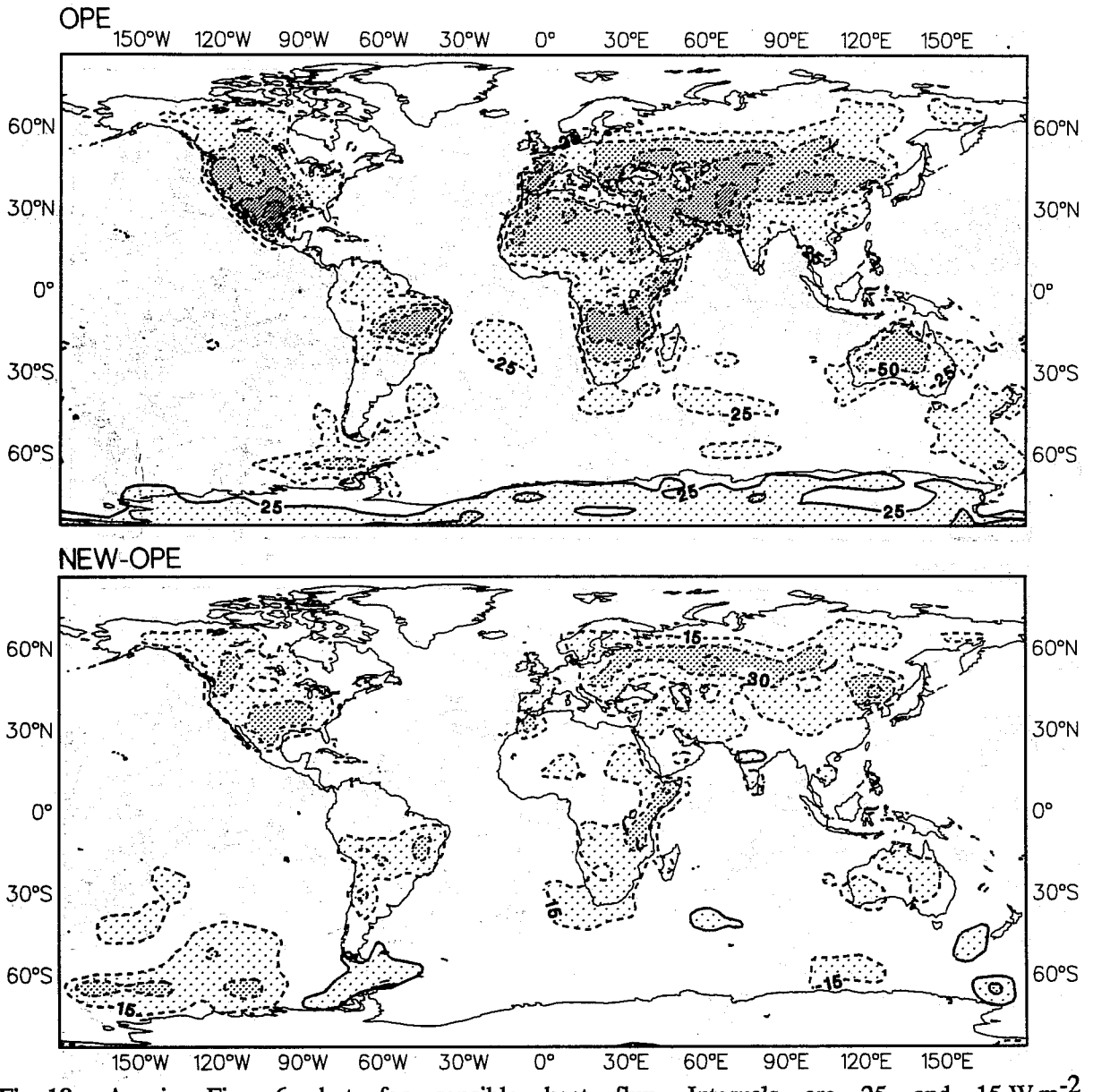

Fig. 10 As in Fig. 6, but for sensible heat flux. Intervals are 25 and 15 W m^{-2}, respectively.

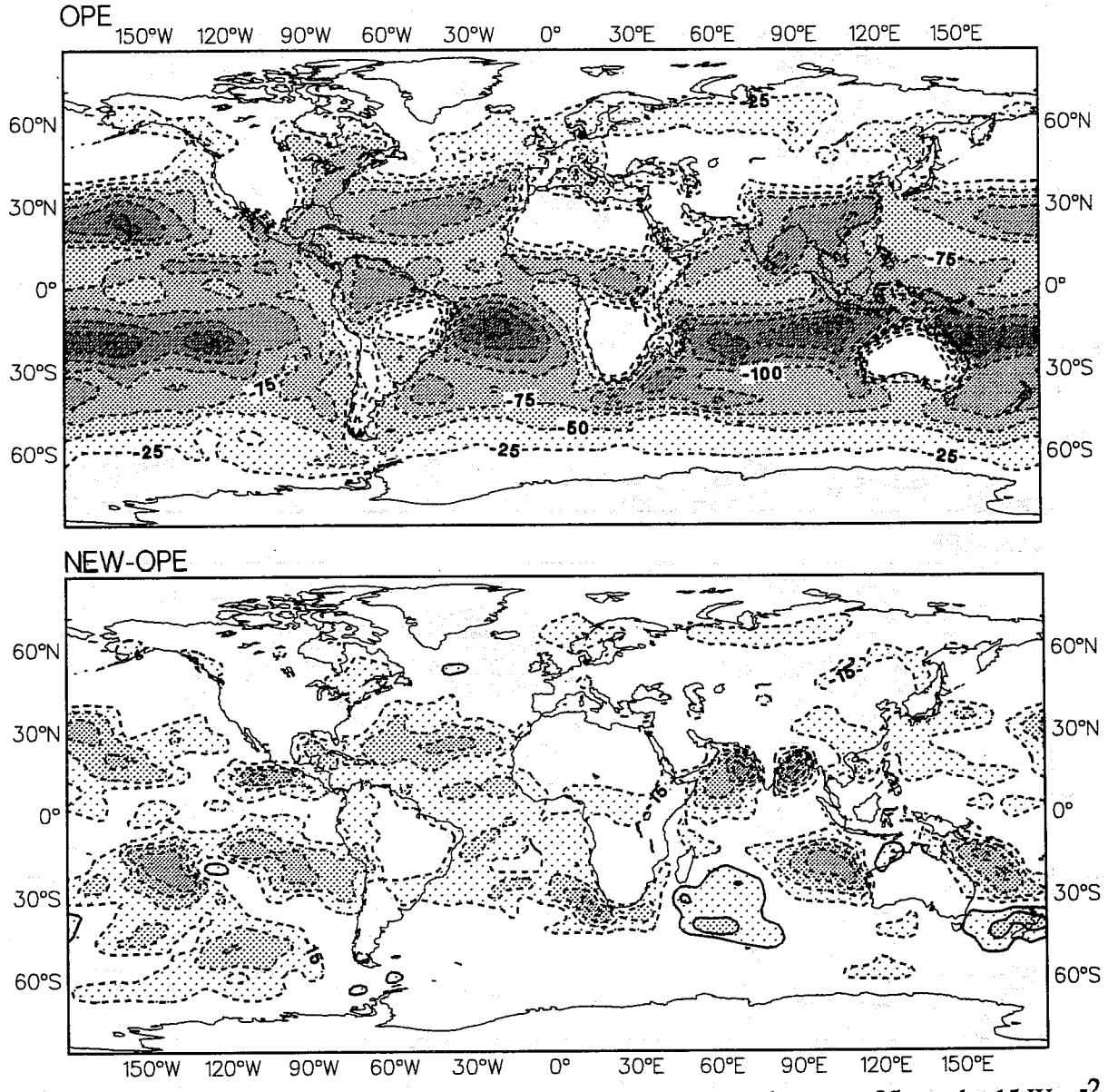

Fig. 11 As in Fig. 6, but for latent heat flux. Intervals are 25 and 15 W m^{-2}, respectively.

3.5 Diabatic heating rates

In the ECMWF model, the sub-grid scale physical processes contributing to the total diabatic heating include the emission-absorption of longwave radiation, the absorption of shortwave radiation, the latent heat release by shallow and deep convective processes and by large-scale condensation, the horizontal and vertical diffusion and, for completeness, the effects of gravity wave drag. Apart from the radiation fields themselves, the largest responses to the change of radiation scheme are found for the heating by deep convection and vertical diffusion. Impact on the representation of the gravity waves is minimal whereas the heating by large-scale condensation is slightly enhanced in the storm track regions of the extratropics. The increase of the sensible heat flux, especially over the continents is reflected by an increase of the heating of the planetary boundary layer by vertical diffusion. Figure 12 present the zonal mean values of the net radiative heating and of the heating by cumulus convection.

The new radiation scheme increases the net radiative cooling in the subtropics, between 700 and 400 hPa, poleward of 30°N and 10°S in the Northern hemisphere summer integration presented. The effect of the cooling by the e-type component of the water vapor continuum can also be seen with NEW in the lowest layers in the tropics. The heating effect of the high and convective cloudiness is clearly seen in the 10°N region with cooling of less than 0.8 K/day in NEW and larger than 1.1 K/day in OPE. In the stratosphere, OPE maintains a +0.50 K/day warming even after more than 60 days of integration, whereas NEW is closer to radiative equilibrium.

The convective activity is clearly enhanced with NEW, with somewhat larger relative cooling of the lower layers and larger heating of the intertropical region. In this NEW simulation, the secondary maxima in convective heating at 28°N and 10°S correspond to more vigourous convection over the Indian monsoon and central Indian Ocean areas as shown in the total precipitation difference map (Fig. 13b). The maxima in convective precipitation over Bangladesh, Sierra Leone, New Guinea, and over the Indian ocean are usually doubled by NEW relative to OPE. This increased convective activity also transports more moisture to the higher layers in the tropics, where areas of relative humidity higher than 80 percent above 300 hPa are more developed with NEW. This increased relative humidity allows for more high-level cloudiness which, through longwave radiative cooling at the top and relative heating at the bottom, contributes to further destabilization of the upper tropospheric tropical layers.

3.6 Temperature profile

One of the clearest effects of the new radiation scheme is the removal of most of the warm temperature bias in the stratosphere. The globally averaged temperature at 30 hPa

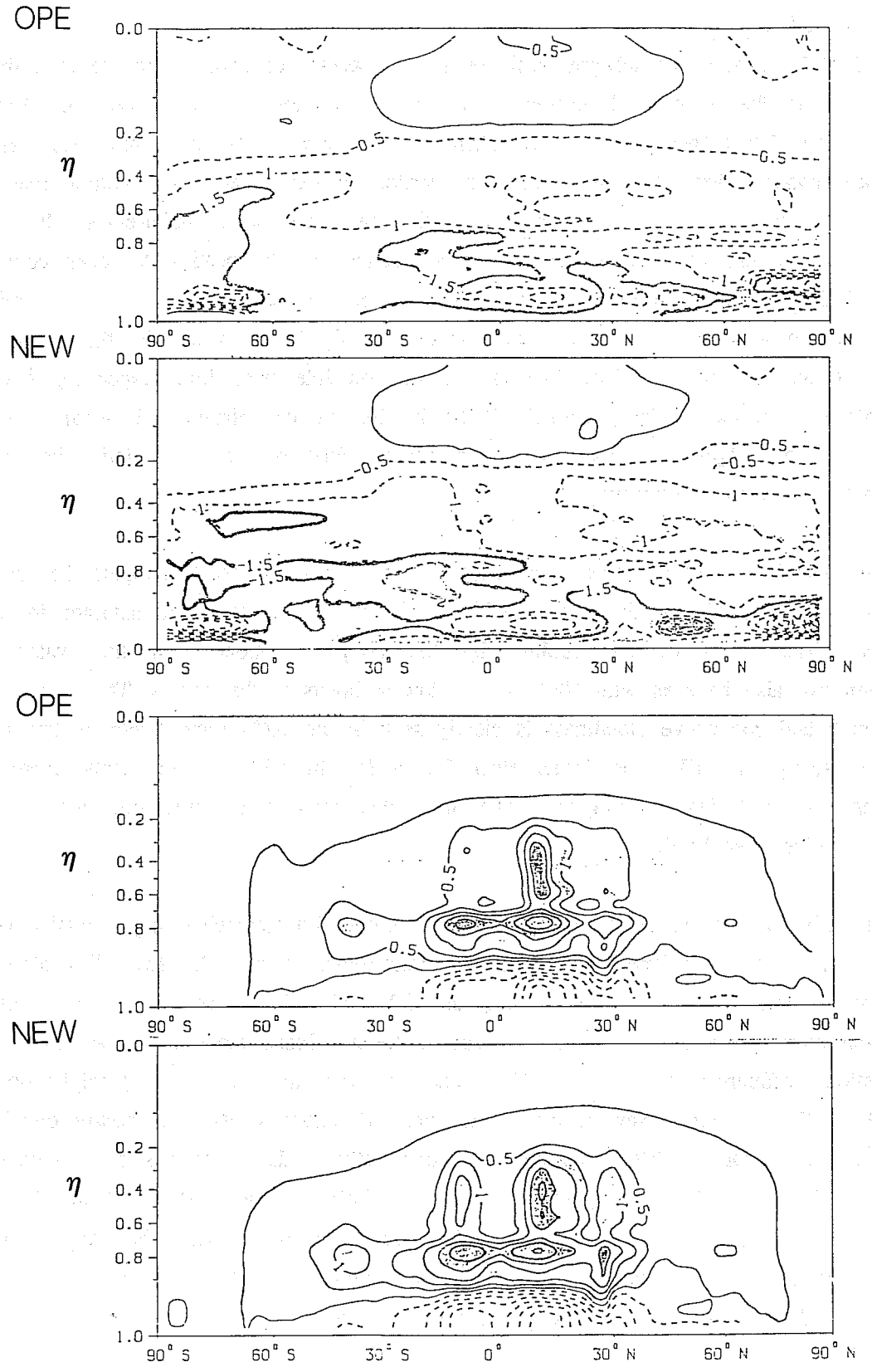

Fig. 12 Contribution of radiation and cumulus convection to the total diabatic heating. From top to bottom, OPE radiative heating, NEW radiative heating, OPE heating by cumulus convection, and NEW heating by cumulus convection. All quantities are in K/day, and correspond to a 30-day average between days 61 and 90 of integrations starting 01.06.87,12Z. Positive quantities between full lines, negative quantities between dash lines.

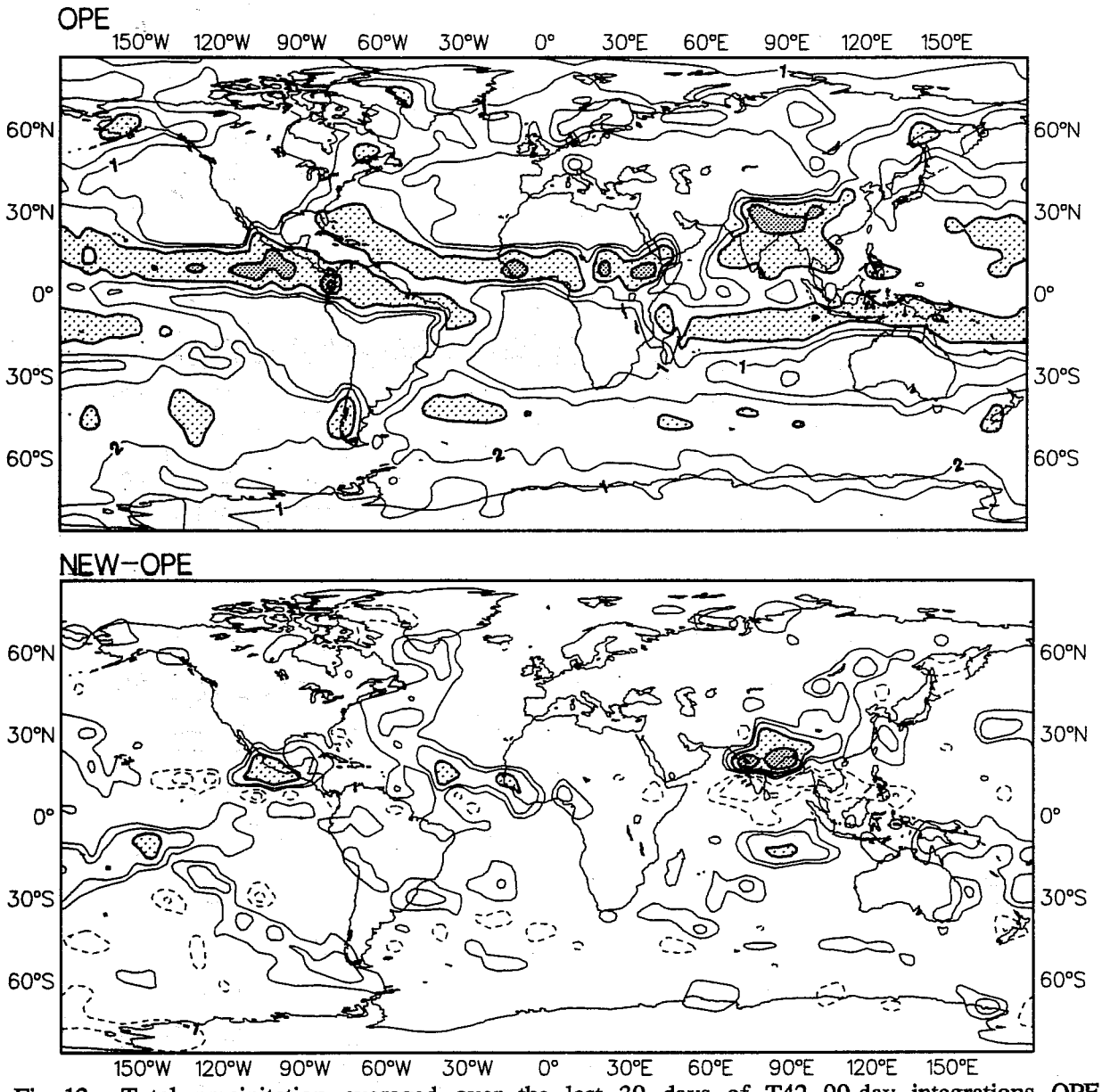

Fig. 13 Total precipitation averaged over the last 30 days of T42 90-day integrations OPE (top) and difference NEW-OPE (bottom). Isolines are for 1, 2, 4, 8, 16 mm/day. Initial date is 01.06.87,12Z.

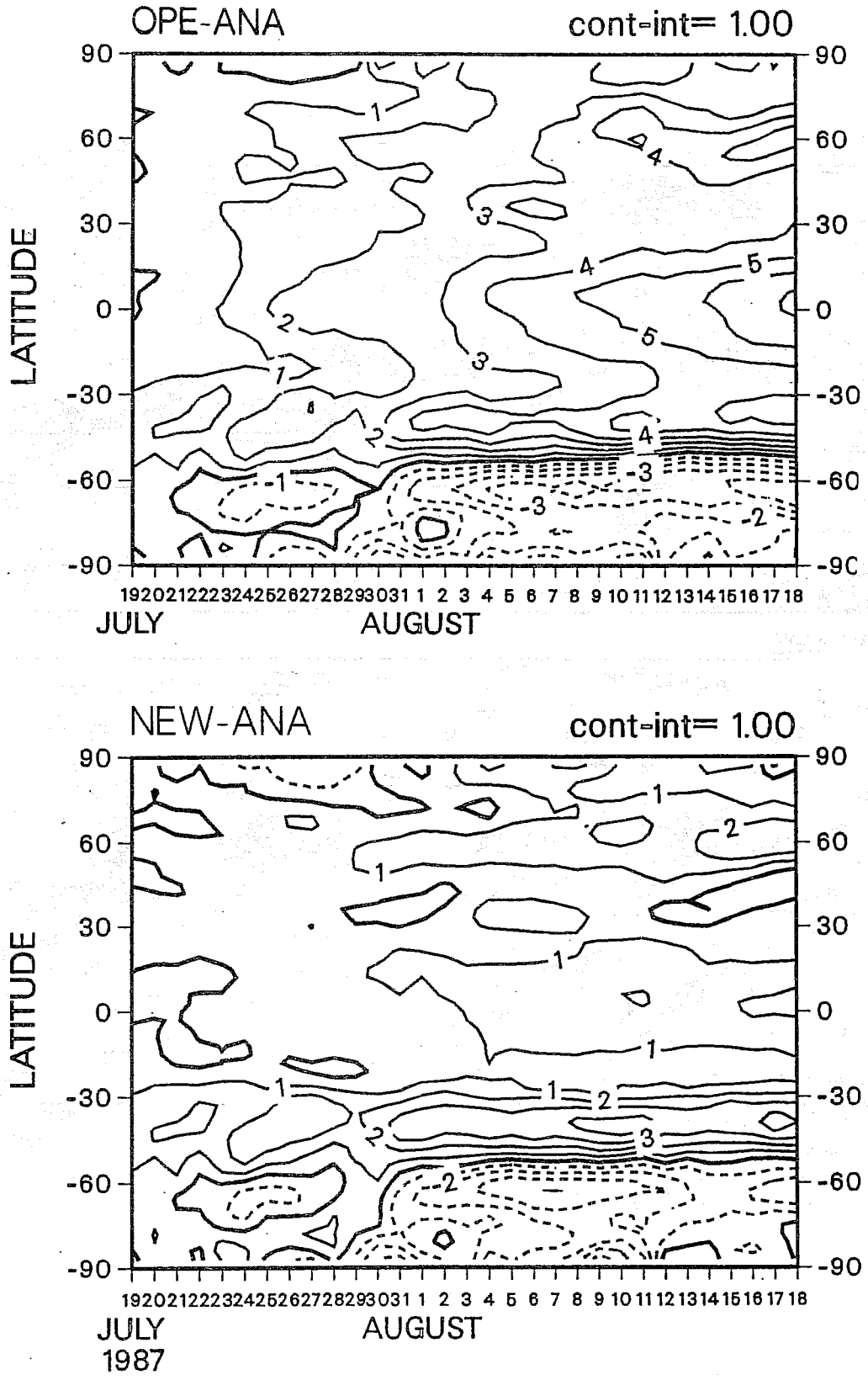

Fig. 14 Error growth of the zonal mean vertically integrated temperature above 100 hPa for T63 30-day integrations starting 19.07.87,12Z with NEW (bottom) and OPE (top). All quantities in degrees.

changes from 233 to 224 K, that at 10 hPa from 245 to 228 K. Figure 14 compares the growth of the temperature error in the lower stratosphere above 100 hPa for two T63 30-day integrations starting 12Z 19/07/87. The improvement is quite clear with reduction of positive errors (model warmer than analysis) by up to 4 K in the equatorial regions, by about 2 K in the Northern hemisphere, and reduction of negative errors by about 1 K poleward of 50°S.

On the other hand, the new radiation scheme increases, by about 2 K, the cold bias in tropospheric temperatures (of about 1 to 2 K) in T42 90-day integrations (Fig. 15). It is important to note that the zonal mean pattern of the temperature error is largely maintained in NEW, so that the impact on the zonal wind error is small (Fig. 16). The relative cooling of the stratosphere improves somewhat the error in zonal wind, but the well documented too strong easterly winds in the high tropical layers appear almost insensitive to the change of radiation scheme.

3.7 Hadley circulation

Numerous diagnostics are available to assess the quality of the representation of the Hadley circulation. Figure 17 compare the errors in vertical velocity in the last 30 days of the winter T42 90-day experiments. The errors in the ITCZ (around 5°S) are decreased by 10 mPa s^{-1} around 200 hPa with similar decrease of errors at higher latitudes. Comparison of the errors in the meridional wind (not shown) also indicates an improved Hadley circulation with a decrease of the error by 0.5 ms^{-1} at 100 hPa on both sides of the core of the ascending branch. Figures 18 shows the analysed, OPE and NEW vertical velocities at different times in the course of a T63 30-day forecast in a 15° zone containing the Southern branch of the Hadley circulation. The systematic drop of the vertical velocity with time displayed in Figs. 18 is a well known systematic error of the model. In that respect, the new radiation scheme does better than the operational scheme, but a sizeable part of the error still remains. Tiedtke and Miller (1988) have shown that these errors are more dependent on the convection parametrization.

3.8 Impact on tropical and extratropical circulations

3.8.1 Tropics

The actual impact of the new radiation scheme on the tropical circulation is difficult to assess as the role of convection is predominant there. The effect of the stronger convective heating on the large-scale flow is most pronounced in the divergent circulation which is stronger with the new radiation scheme. This is evident in the zonal mean (Fig. 17) and in the geographical distribution of the circulation as is evidenced in the velocity potential at 200 hPa. The new radiation scheme strengthens the large-scale circulation and thus gives a somewhat better agreement with the analysed field. However, the basic errors characteristic

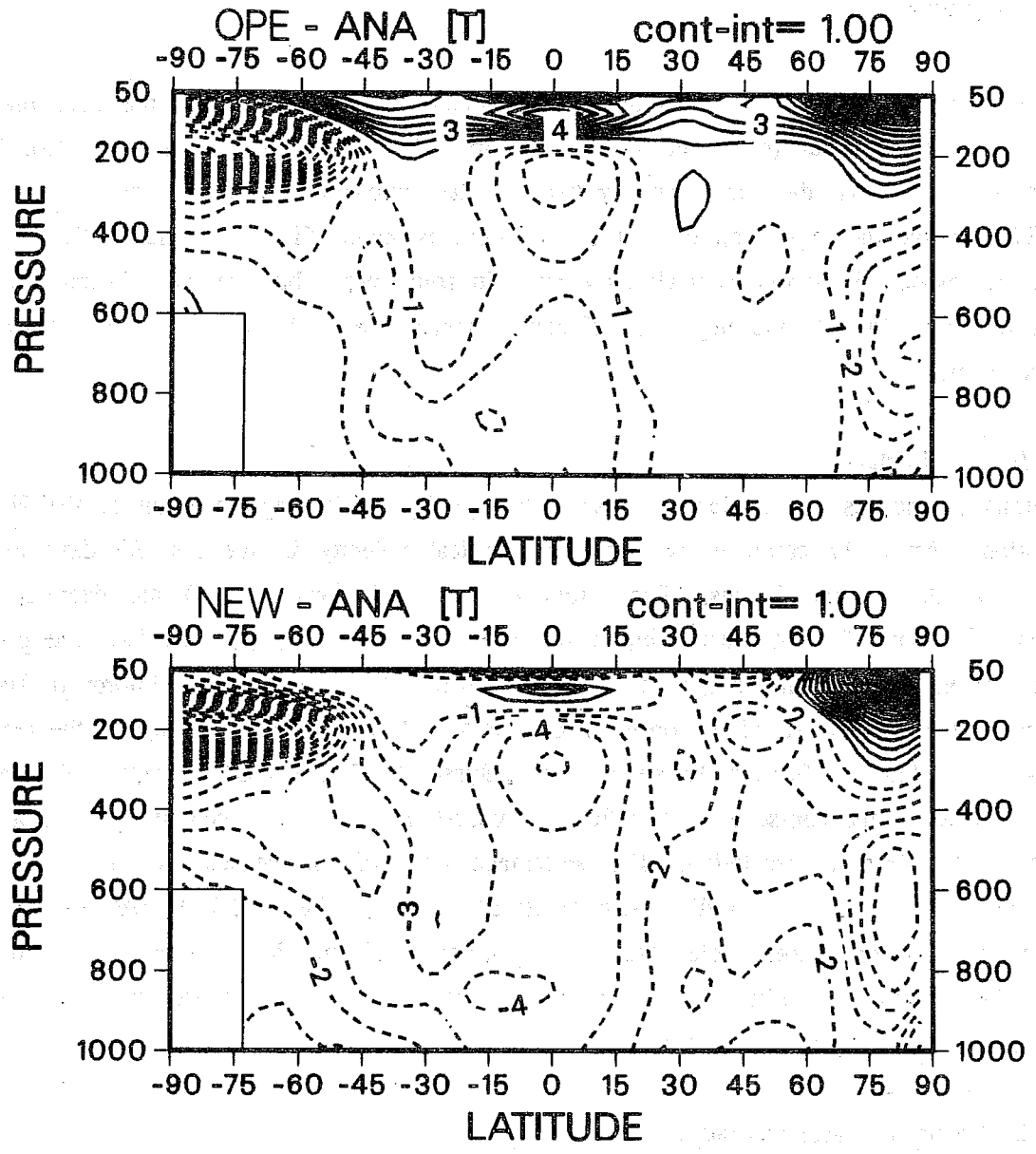

Fig. 15 Zonal mean temperature errors for day 61-90 for T42 winter simulations with NEW (bottom) and OPE (top). Initial date is 01.12.87,12Z.

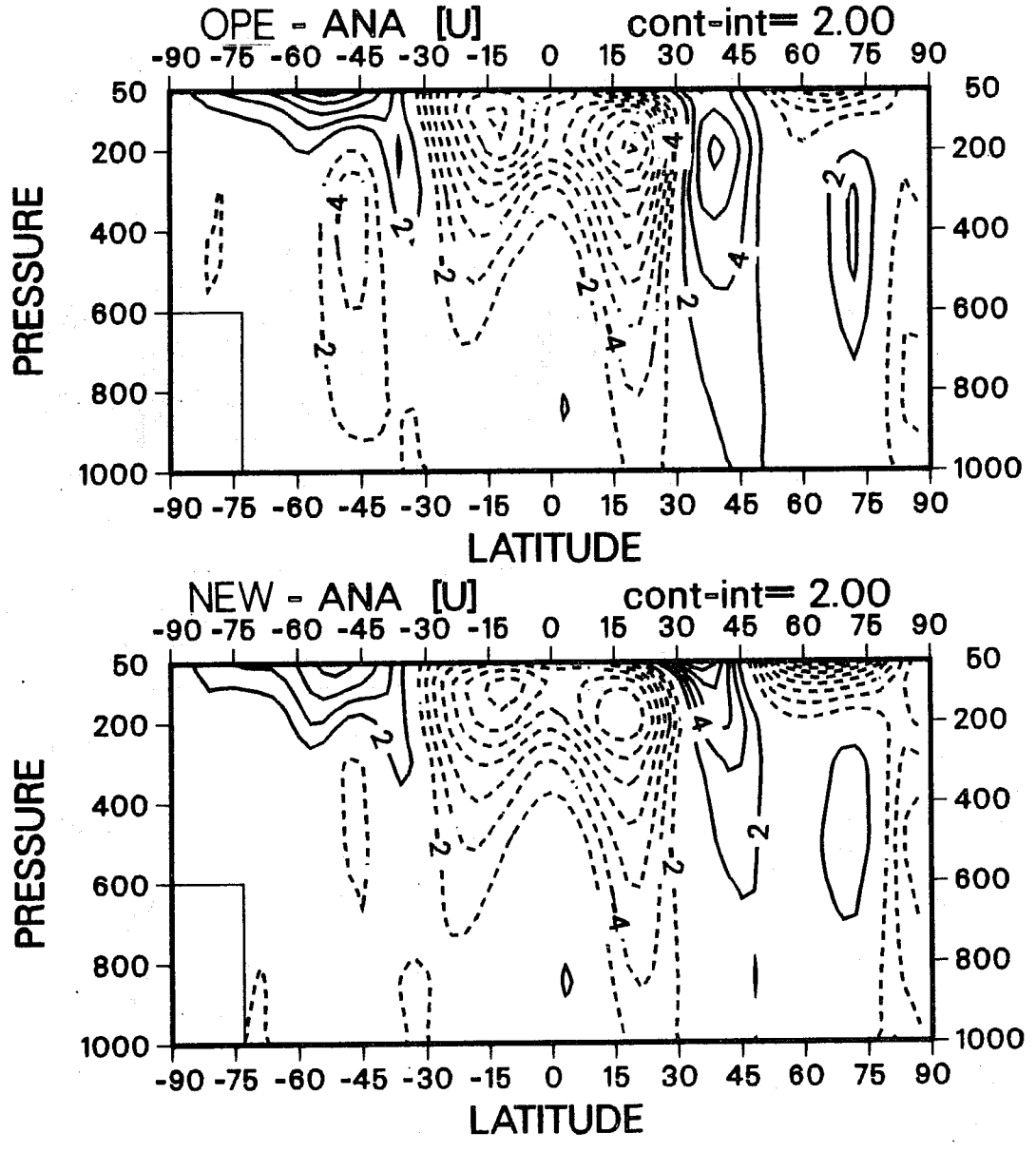

Fig. 16 As in Fig. 15, but for zonal wind (m s^{-1}).

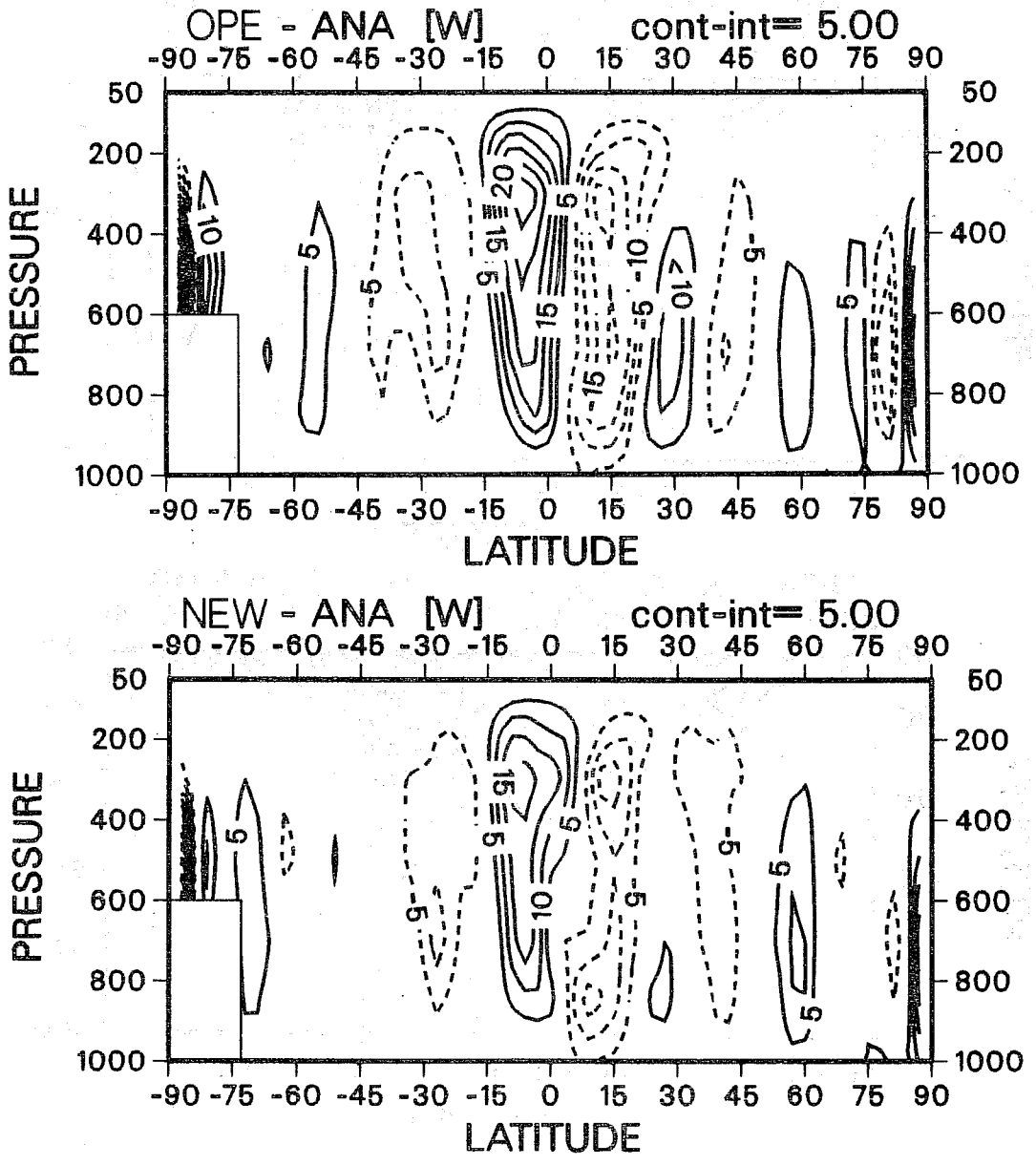

Fig. 17 As in Fig. 15, but for vertical velocity (10 Pa^{-3} s^{-1}).

of the operational model are still present: One can notice the collapse of the circulation over the Indonesian area and the West Pacific present for either radiation scheme. Experiments with different convection schemes (Tiedtke and Miller, 1988) have shown this feature to be closely related to deficiencies in the Kuo onvection parametrization, which was operational at the time, which underestimates the heating in the higher tropical troposphere.

The rotational flow is also affected but to a smaller extent. Indirect confirmation is found in the zonal mean flow errors which are hardly affected by the change of radiation scheme.

3.8.2 Extratropics

In the long-range, the new radiation scheme brings some improvements to the representation of the mean circulation in the extratropics of both hemispheres. In Figure 19, the geopotential height error at 500 hPa averaged over the last 30 days of T42 90-day integrations is shown for OPE and NEW. On the short and medium range of the forecasts, it is more difficult to understand how a change in the physical parametrization schemes which affects primarily the tropics, influences the quality of individual extratropical forecasts. For this it is useful to study the impact as illustrated by objective scores of an ensemble of forecasts. For an ensemble of 19 pairs of T63 10-day forecasts spanning the period April 1987 - October 1988, the anomaly correlations of geopotential height for the 1000-200 hPa layer (Fig. 20) show the larger impact in the medium-range in both hemispheres with the new radiation scheme. However, from the scatter of the anomaly correlation for the predicted height fields (Fig. 21), it is evident that the forecast quality diverges with forecast time and is deteriorated in a number of forecasts. In view of the results of predictability and forecast spread studies, this is not too surprising. As forecasts lose forecast skill in locating low-frequency long-wave patterns, which in turn define the storm tracks, improving diabatic forcing does not necessarily gain forecast skill. It can even achieve the opposite, especially when the models level of eddy activity is increased as it is the case in these experiments (see 4.4). However, the impact of the new radiation scheme is positive at all wavenumbers in the Southern hemisphere, and for wavenumbers 1 to 3 in the Northern hemisphere. Much of the deterioration comes from the short synoptic waves.

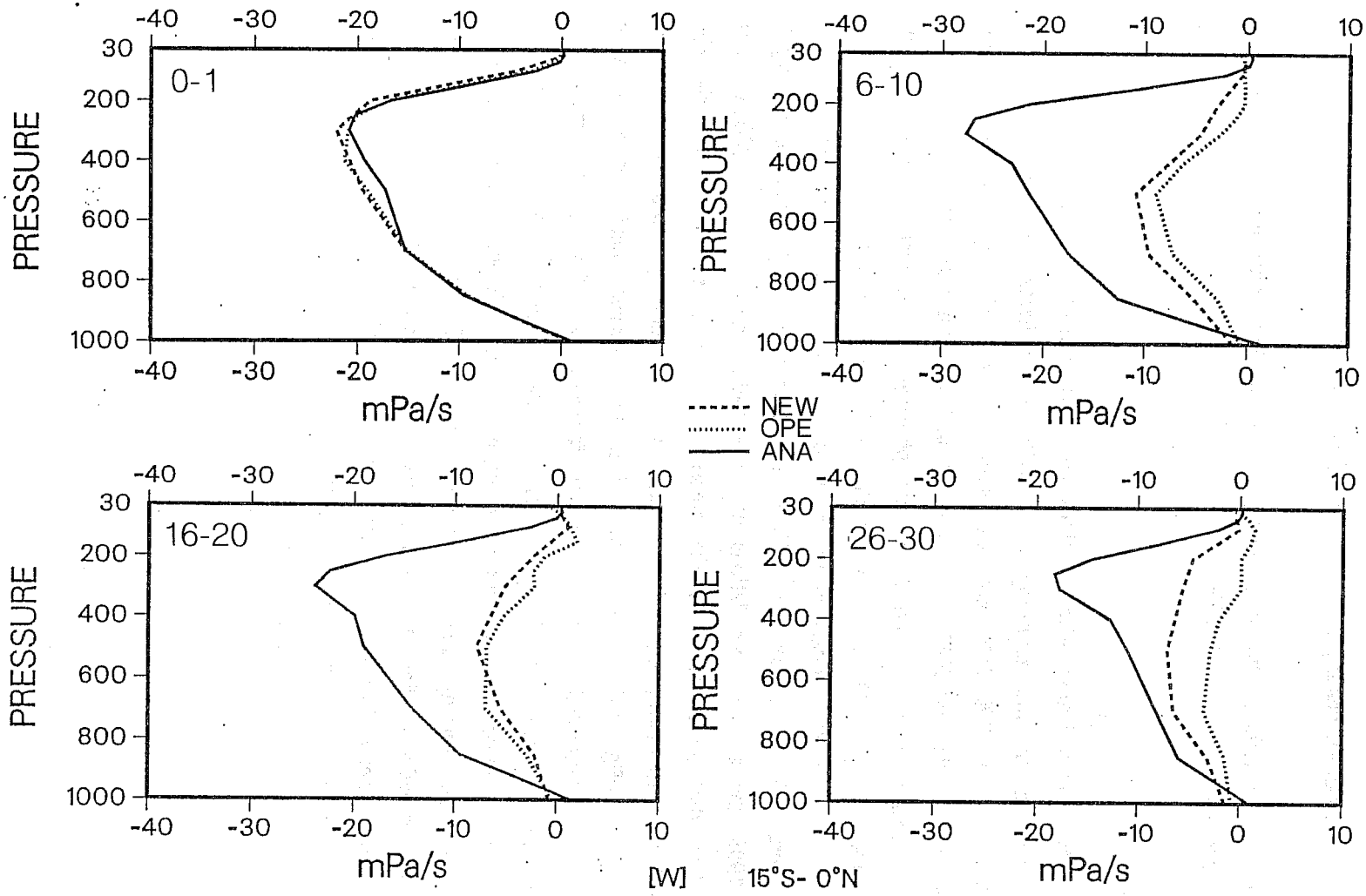

Fig. 18 Profile of the vertical velocity averaged over the 0°-15°S zonal band as given by the analysis (full line) and the forecast model with OPE (dotted line) or NEW (dash line) for different periods within a T63 30-day forecast starting 17.01.89,12Z. Top left is the average between days 0 and 1, top right between days 6 and 10, bottom left between days 16 and 20, bottom right between days 26 and 30.

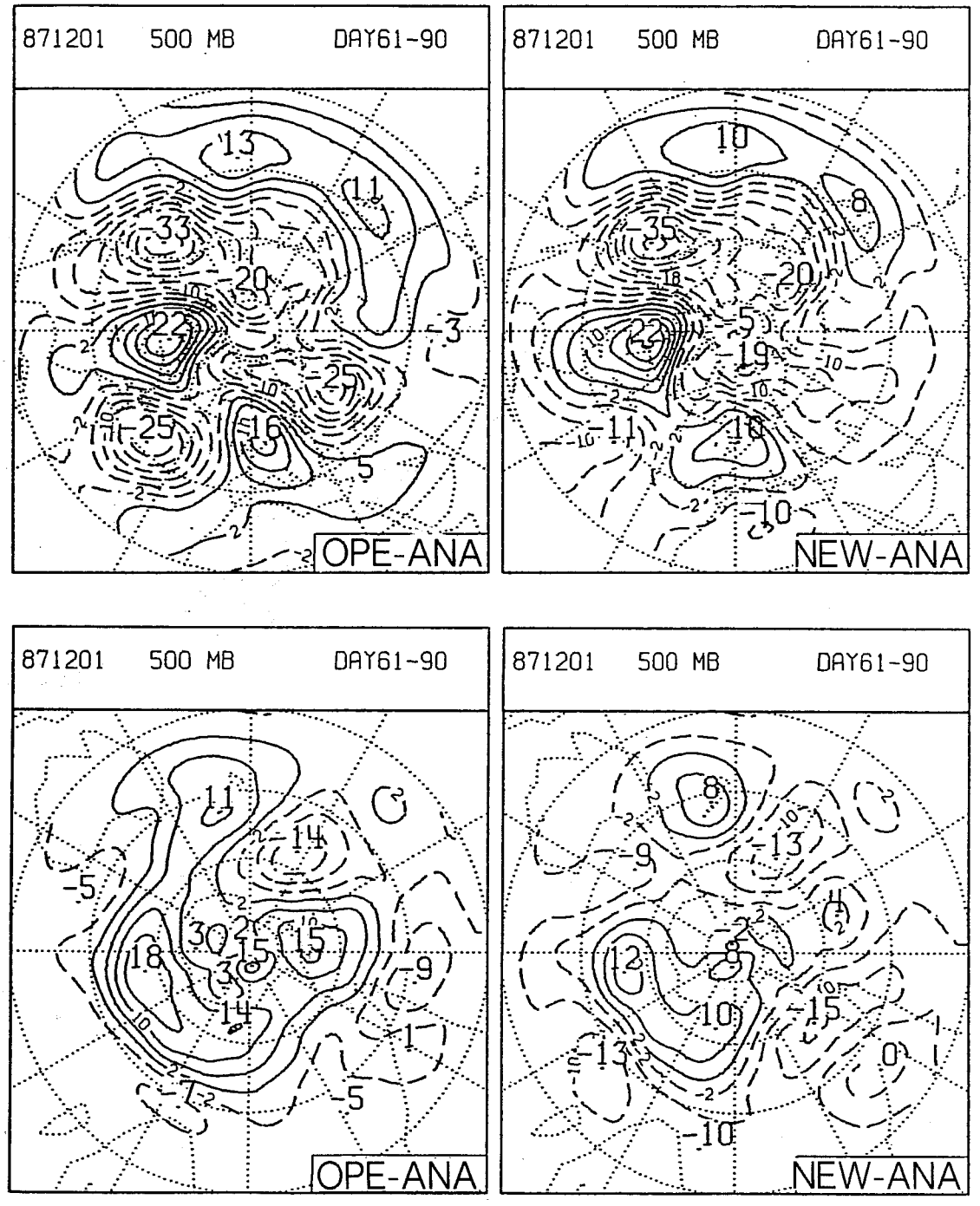

Fig. 19 Errors in geopotential height field in the Northern and Southern hemispheres at 500 hPa averaged over the last 30 days of T42 90-day integrations with OPE (left) and NEW (right).

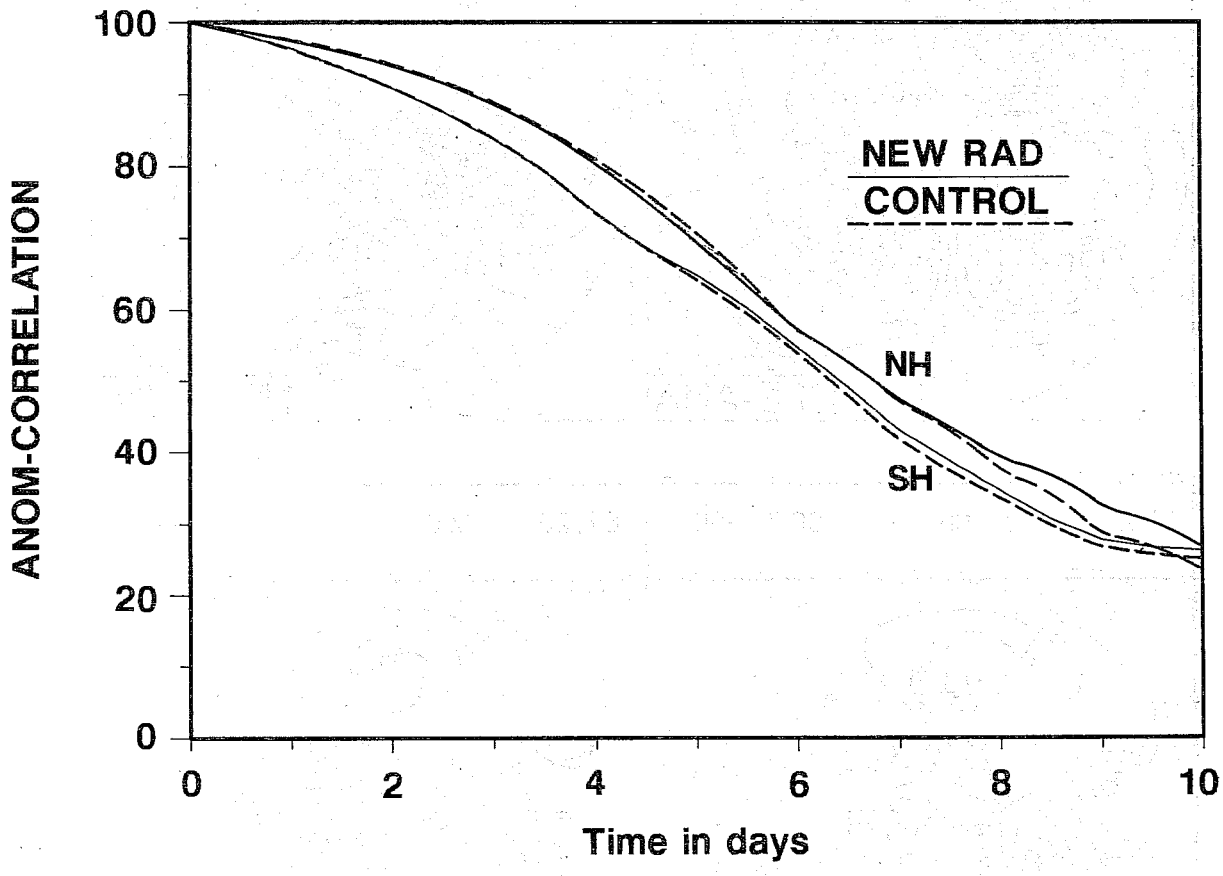

Fig. 20 Mean anomaly correlation of 1000-200 hPa heights in extratropical Northern and Southern hemispheres for 19 T63 10-day forecasts with NEW (full line) and OPE (dashed line).

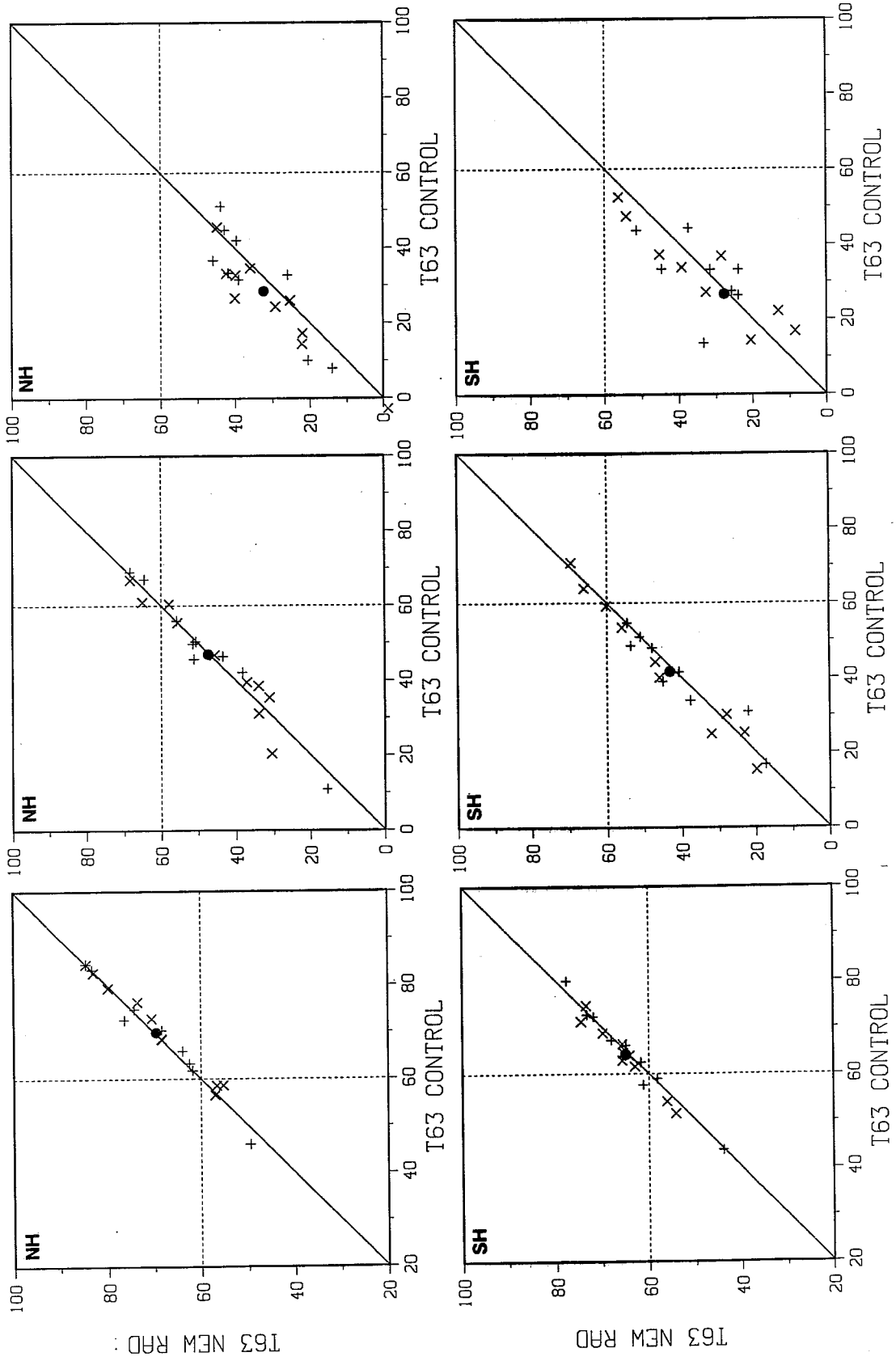

Fig. 21 Scatter of the anomaly correlation of 1000-200 hPa heights in extratropical Northern and Southern hemispheres at days 5, 7 and 9 for an ensemble of 19 T63 10-day forecasts. Improvement appears as a point above the line of slope 1.

4. DISCUSSION

Three features distinguish the new radiation scheme from the operational scheme, namely the increased clear-sky net radiative cooling, the increased net radiation available at the surface in clear-sky conditions, and the larger radiative impact of the cloudiness. Their direct impact is seen in the decrease in the stratospheric temperature bias and the improved level of the OLR. However, most of the other effects described in the preceding section are the results of more indirect responses to the change in the radiation transfer scheme. Here we discuss the global energy budget, the tropical circulation, the cloud-radiation interaction and the energy cycle of the model on a more synthetic basis.

4.1 Energy budget considerations

To put the results discussed above in perspective, we first consider the magnitude of the change that the new radiation scheme has brought about in the global energy balance of the model. From a set of 12 pairs of T63 10-day experiments starting at the 15th of each month between 15 May 1987 and 15 April 1988, a pseudo mean annual energy budget has been computed from the averages over the last 5 days of the forecasts. This is displayed in Figure 22. Although this approach does not give a picture of the model's real energy balance, that would be obtained if it were integrated over at least one annual cycle, it allows a simple illustration of how the forcing mechanisms have changed. The main difference between NEW and OPE is seen for the solar radiation absorbed by the atmosphere (from 85 to 66 Wm^{-2}). The decrease in clear-sky shortwave absorption is seen in global mean values indicating that the presence of clouds (which varies from 0.488 in OPE to 0.508 in NEW) has not substantially modified the forcing (a decrease of about 20 percent of the clear-sky shortwave absorption). In contrast, the increase in clear-sky longwave cooling (of about 12 percent, seen in instantaneous one-dimensional calculations) is partly compensated by the heating below the more radiatively active high-level cloudiness in the tropics and the atmospheric loss by longwave radiation only increases from 171 to 177 Wm^{-2}. At the surface, the net total radiation increases from 87 to 117 Wm^{-2}. The change of radiation scheme thus has a large impact: the overall net atmospheric cooling changes by more than 30 percent from 86 to 116 Wm^{-2} from 0.74 to 0.95 K/day.

This effect is even larger in the tropics. There, the mean annual net heating of about 60 Wm^{-2} is the sum of a 320 Wm^{-2} heating by absorption of solar radiation and a 260 Wm^{-2} cooling by longwave emission. The main point, stressed by Ramanathan (1986) is that this net heating of only about 20 percent of the absorbed solar radiation (with the remaining 80 percent heating the tropical surface) is the driving force for the general circulation of the atmosphere and the ocean. Therefore, a change of 10 percent in the column absorbed solar radiation or in the longwave emission would potentially translate into a factor of five increase in that driving force or likewise in the required poleward transport of heat. In addition, as

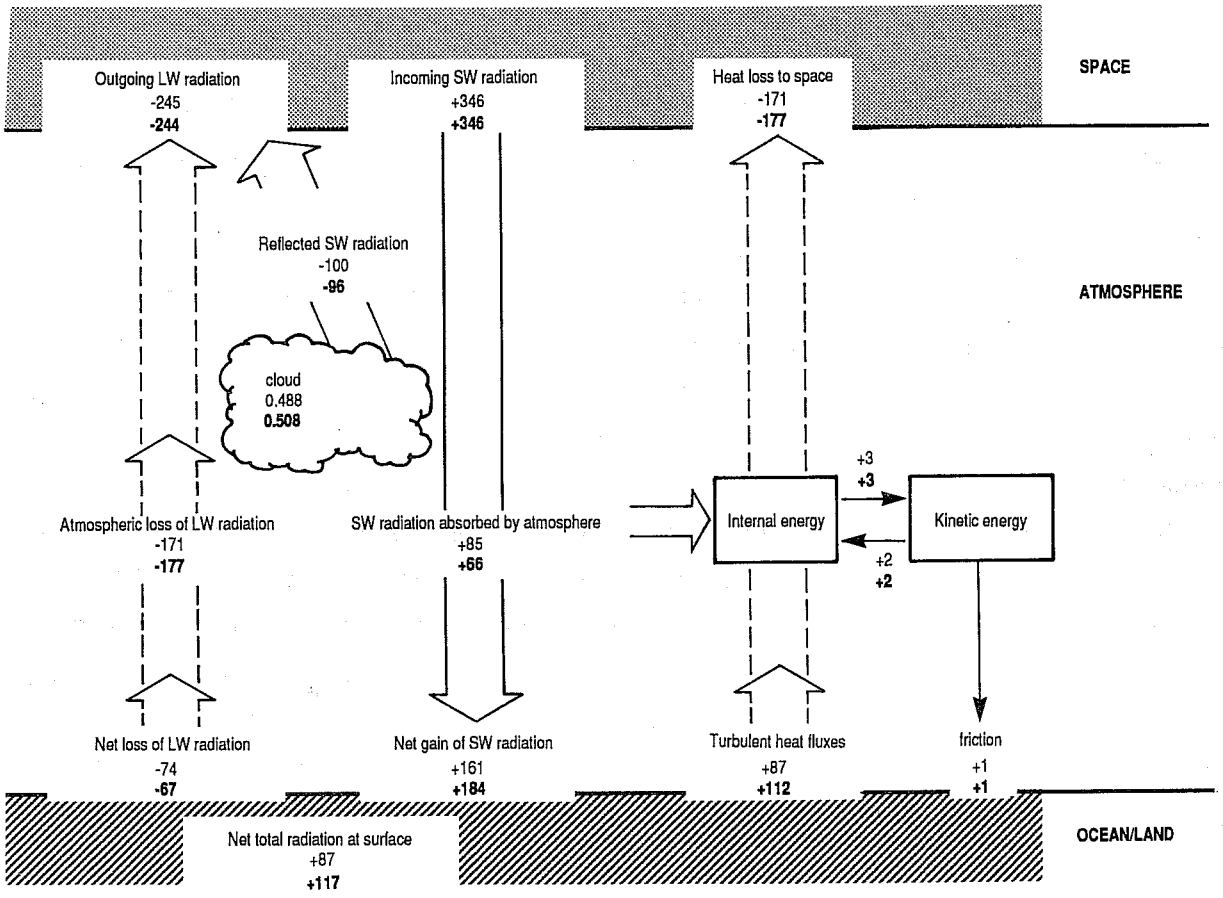

Fig. 22 The energy balance of the ECMWF model with OPE (top) and NEW (bottom). All quantities in W m^{-2}, except the fractional cloudiness.

a whole the troposphere is subject to a net radiative cooling (of about 100 Wm^{-2}) whereas the surface is subject to a net radiative heating of the same amplitude. The change of radiation scheme emphasizes this contrast, which destabilizes the troposphere and provides the fundamental source for the enhanced tropospheric convection.

4.2 Tropical circulation

The results in the tropics can be explained following the approach presented by Betts and Ridgway (1988) after arguments first proposed by Riehl and co-workers (1957, 1979). In this approach one considers an idealized energy balance model of the steady-state tropical circulation over the uniform ocean surface that links the tropospheric net radiative cooling, the surface fluxes and the mean subsidence in the descending branch of the Hadley circulation (the regions of deep precipitating convection occupy only a small fraction of the tropics). In this simplified description which neglects horizontal advection and the atmospheric export of heat to higher latitudes, the surface evaporation is coupled to the ascending mass flux in the ITCZ and the compensating subsidence in the descending branch where the surface fluxes compensate the integrated radiative cooling. In this framework, the increased radiative cooling given by the new radiation scheme is compensated by an increase in evaporation; this extra humidity is transported in the PBL into the ITCZ where it feeds the enhanced convection. The air ascends to exit near the tropopause and gives more convective precipitation. The outflow then descends as a result of radiative cooling, with enhanced subsidence. This simple model is consistent with the results obtained in section 3 which show larger latent fluxes over the oceanic subtropics, increase in heating by cumulus convection and in convective precipitation in the ITCZ and a stronger Hadley circulation.

Globally, the changes in mean radiative heating are largely compensated for by changes in the mean convective profiles. Although for different experiments (their initial modification of the convective heating profiles was compensated for by changes in radiative heating), these results corroborate the findings of Albrecht et al. (1986) that the problems of the parametrization of cumulus convection and of cloud-radiation interactions are intricately coupled.

4.3 Cloud-radiation interactions

Experiments by Ramanathan et al. (1983) and Slingo and Slingo (1988) have shown that cloud-radiative effects have the potential to influence significantly the tropical thermal structure, the mid-latitude westerlies, and regional phenomena such as the monsoon. In particular, Ramanathan et al. (1983) have compared the circulations produced by the same model including either optically thick (black) or transparent cirrus clouds. The black

clouds provided a strong meridional gradient in the upper level radiative heating fields, from a strong local upper level heating as well as a column heating in the tropics to a strong local upper level cooling at polar latitudes. Thus an enhancement of the zonal winds resulted from the intensified equator-pole temperature gradients.

Our results do not show such an effect although the new scheme makes the high clouds much more opaque in the longwave. Most of the experiments with the new radiation scheme show an increase of the zonal mean temperature error by 1 to 2 K over a wide fraction of the atmosphere. This shift in the mean temperature is not accompanied by any significant change in the meridional temperature gradient. In the tropics, the more radiatively active high-level cloudiness with the new scheme is a local heat source which contributes to a destabilization of the upper troposphere and thus leads to rising motion and upper-level mass divergence. However, this enhanced tropical diabatic heating is compensated for by stronger eddy meridional transport which explains the small impact on the meridional temperature gradient and the mean zonal winds.

In our integrations with the new radiation scheme, the cloudiness remains relatively stable with respect to its distribution in the control integrations. The total cloud cover generally increases by 2-3 percent in the long T42 90-day integrations with a slight upward shift towards higher-level clouds in the tropics, but no drastic change in the vertical or geographical distribution in the extratropics. Even smaller variations are seen in the T63 and T106 10-day forecasts. Thus the change seen in the height anomaly correlation of Fig. 20 can mainly be related to the effect of the new radiation scheme and cloud optical properties. Figure 21 also show that the impact on any individual forecast (either beneficial or detrimental) is generally large, usually larger than the impact found by Slingo (1987) for a change of cloud prediction scheme. We can therefore somewhat revise her conclusion "that, for a forecast model, cloud prediction can be at least as important as the parametrization of the radiation transfer". At the time of her experiments, the ECMWF model may have shown a larger sensitivity to cloud distribution than to radiation transfer just because the radiation experimentation (carried out to support the implementation of the 1984 version of the ECMWF radiation scheme (OPE)) was carried out with a cloud scheme (Geleyn et al., 1982) which gave little geographical and vertical contrast in the cloudiness distribution, and because the cloud experimentation (carried out to support the operational implementation of the 1985 version of the ECMWF cloud scheme) was performed using a radiation scheme (Ritter, 1984) which strongly underestimated the differential radiative heating due to the presence of clouds.

4.4 Eddy activity

As discussed by Arpe (1988), one of the systematic errors of the ECMWF model is the drop of eddy energy (eddy available AE and eddy kinetic KE) and increase of zonal energy (zonal available AZ and zonal kinetic KZ) during the course of the forecasts. According to Arpe (1988), this feature is mainly related to the reduction of the transient waves as the standing waves contribute little to the total eddy energy.

Together with latent heat release and sensible heat transfer, radiation produces differential heating and thus generates available potential energy. Compared with the operational scheme, the new radiation scheme increases the contrast between the tropics, where local relative radiative heating is now found under the more radiatively active high-level cloudiness, and the subtropics where a larger clear-sky radiative cooling prevails. This effect is further enhanced by the increase in latent heat release in the tropics. As seen in Table 5, the effect of the more realistic net radiative cooling of the new radiation scheme is to give the model an enhanced energy cycle, at all wavenumbers, initially and in long integrations. In that respect, the new radiation corrects at least partly the problem mentioned above. A higher level of eddy activity is obtained through (i) an increase in GZ, the generation of AZ, (ii) a higher AZ (now in good agreement with its analysed value), (iii) an increase in CA, the conversion between AZ and AE, (iv) a higher AE (in better agreement with its analysed value), (v) an increase in CE, the conversion between AE and KE. The improvements are clear in terms of both the latitudinal distribution of AE and KE (Fig. 23) and of their temporal evolution.

Results of the experimentation discussed above also show that the new radiation scheme contributes to a partial correction of some errors of the ECMWF model. The weakening of the trade winds and the weakening of the transients in both tropical and extratropical latitudes are much reduced. The new scheme also increases the low frequency variability (periods greater than 5 days) of the model. As far as a cloud-radiation interaction mechanism is concerned (Ramanathan, 1986), the new scheme should also make the model more sensitive to tropical SST anomalies.

Table 5

Box diagram of the energy cycle of the model averaged over the last 30 days of T42 90-day integrations with OPE and NEW. First panel is the corresponding analysed values. Initial date is 1.12.87,12Z.

Energy terms are in kJ m^{-2}, conversion terms in Wm^{-2}.

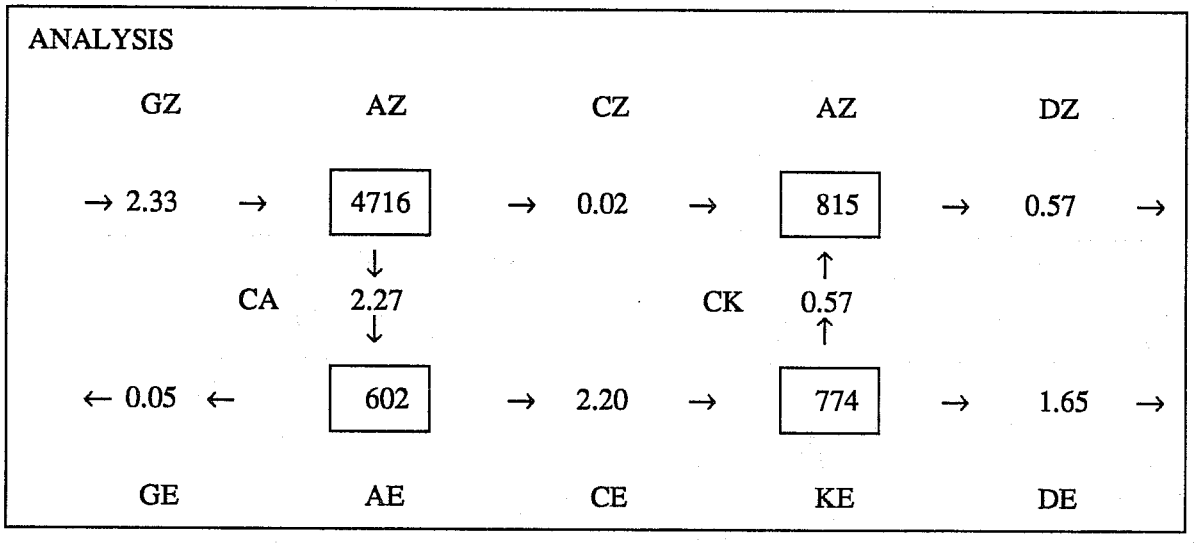

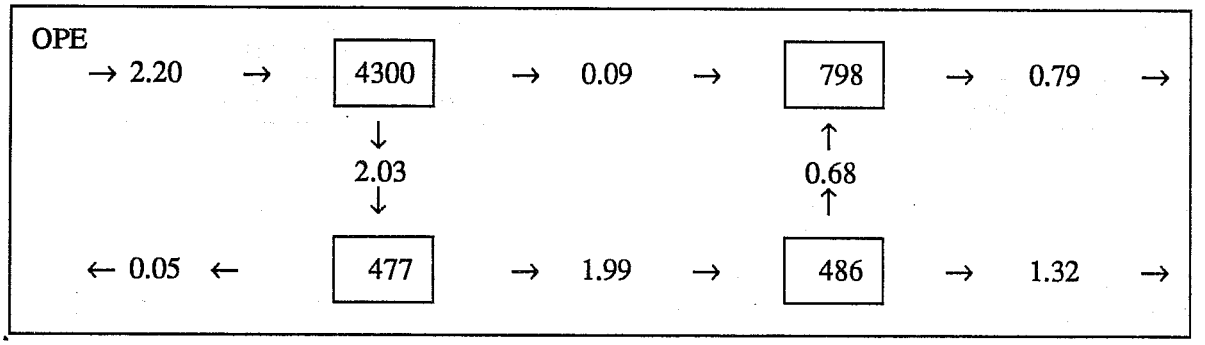

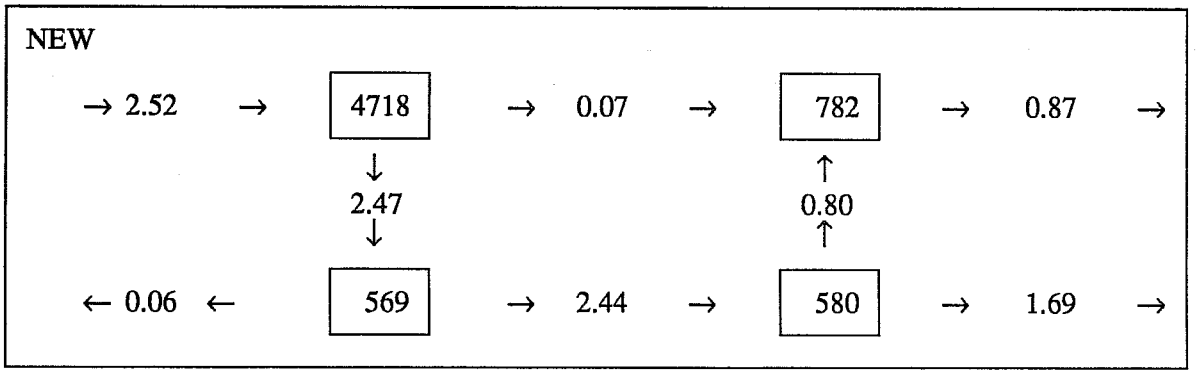

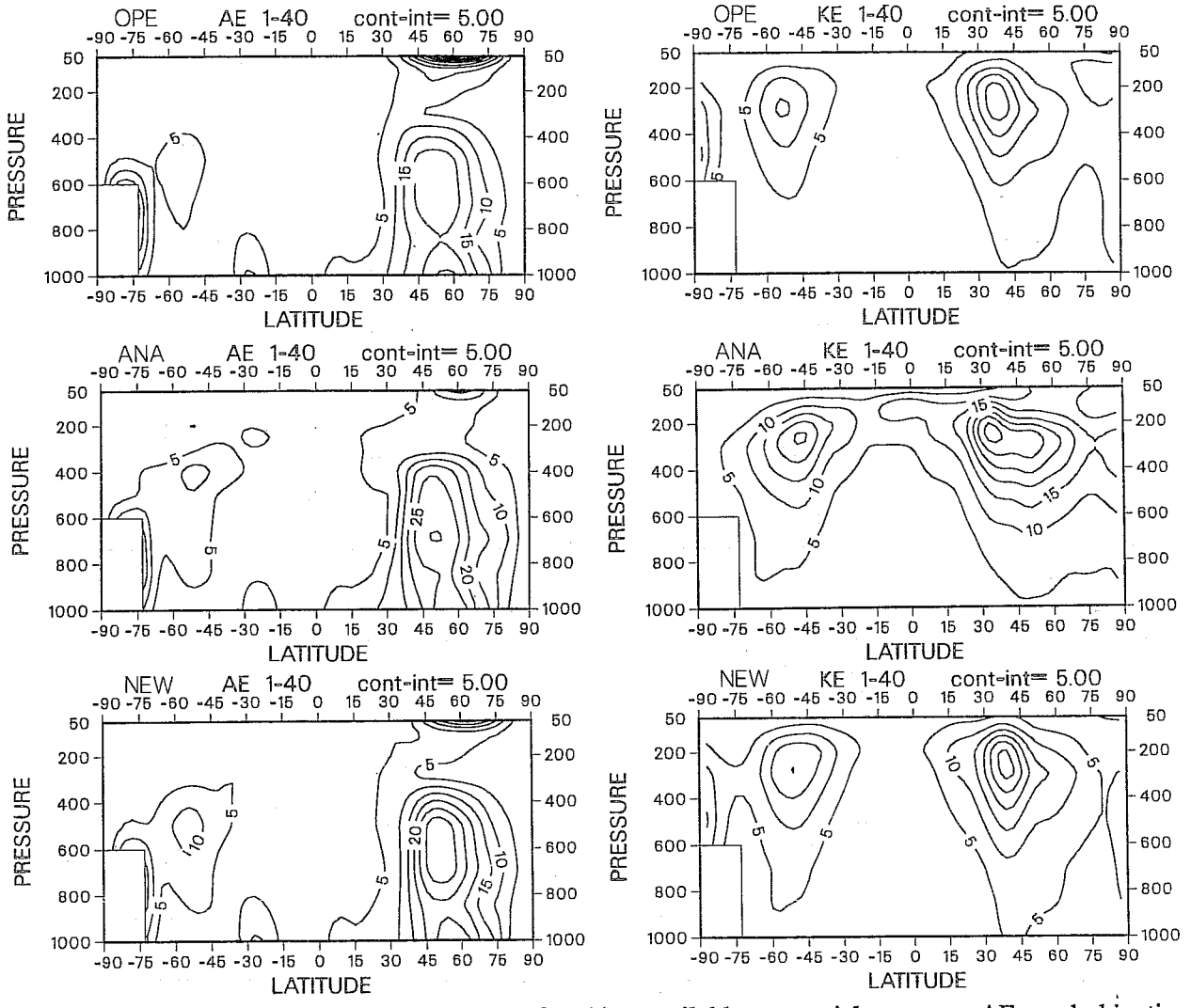

Fig. 23 The zonal mean distribution of eddy available potential energy AE and kinetic energy KE averaged over the last 30 days of T42 90-day integrations with OPE (top) and NEW (bottom) radiation schemes. Middle panel is the corresponding analysis.

5. CONCLUDING REMARKS

Among all sub-grid processes whose effects have to be parametrized in a large-scale numerical model of the atmosphere, radiation transfer is a physical process for which there is a relatively firm physical basis. A theoretical description of radiation transfer has been known for decades. Compilations of spectroscopic parameters for the most important radiatively active constituents of the atmosphere are available. Very accurate models such as the line-by-line models can be used to compute reference values of the clear-sky fluxes and, in its development, the new radiation scheme has been carefully checked against such accurate models for both the longwave (Scott and Chédin, 1981; Morcrette and Fouquart, 1985) and shortwave ranges.

This paper summarizes the results from a large number of integrations that have been performed using the operational radiation scheme and the revised radiation scheme. The direct impact of the new scheme produces:

(i) more realistic radiative flux divergences, which are underestimated in the operational scheme and as result, the model becomes more active;

(ii) more accurate outgoing longwave radiation at the top of the atmosphere, most noticeable in areas of tropical convection due to a more realistic radiative response to clouds; this feature is of particular importance for verification against satellite observations;

(iii) increased solar radiation at the surface, this is significant for predicting surface temperatures over land and for the thermal forcing by land-sea contrast.

The new radiation scheme also contributes partial corrections through various interactions to a number of systematic errors of the ECMWF model and as such the introduction of this radiation scheme in the ECMWF operational forecast system has had impact on the analyses through the first guess. From the comparisons discussed above, it is likely to affect the divergent flow (as Trenberth and Olson, 1988, pointed out for previous changes in the ECMWF forecasting system), but also the surface fields. These changes are of importance for ocean modellers who use those fields as a forcing for their models (Simonot and Le Treut, 1987).

The new radiation scheme, which has become the operational ECMWF radiation scheme on 2 May 1989, corrects for many of the known deficiencies in the present radiative parametrization. However, improvements of this new scheme are still possible. They are likely to come from

(i) a better knowledge of spectroscopic parameters, continuum, line shapes and intensities which should lead to a better representation of clear-sky fluxes;

(ii) in-situ quality measurements of the surface fluxes with high spectral resolution which should help validate the line-by-line models against which the new radiation scheme was calibrated;

(iii) an extensive use of satellite data (such as ISCCP, ERBE), to document more precisely cloud fields and their radiative impact on various time and space scales; this will improve the parametrization of clouds and cloud-radiation interaction which is the weakest part in radiation parametrization.

REFERENCES

Albrecht, B.A., V. Ramanathan, and B.A. Boville, 1986: The effects of cumulus moisture transport on the simulation of climate with a general circulation model. J. Atmos. Sci., 43, 2443-2462.

Arpe, K., 1988: Planetary-scale diabatic forcing errors in the ECMWF model. ECMWF Workshop on Diabatic Forcing, 30 Nov.-3 Dec.1987, ECMWF, Reading, U.K., 103-150.

Arpe, K., and E. Klinker, 1986: Systematic errors of the ECMWF forecasting model in mid-latitudes. Quart. J. Roy. Meteor. Soc., 112, 181-202.

Arpe K., and S.K. Esbensen, 1989: Surface stresses and latent heat fluxes over oceans in short range forecasts: Their annual and interannual variability and comparison with climatological estimates. Annalen der Meteorologie (Neue Folge).

Betts, A.K., and W. Ridgway, 1988: Coupling of the radiative, convective, and surface fluxes over the Equatorial Pacific. J. Atmos. Sci., 45, 522-536.

Bonnel, B., Y. Fouquart, J.-C. Vanhoutte, C. Fravalo, and R. Rosset, 1983: Radiative properties of some african and mid-latitude stratocumulus clouds. Beitr. Phys. Atmosph., 56, 409-428.

Brankovic, C., 1986: Zonal diagnostics of the ECMWF 1984- 85 operational analyses and forecasts. ECMWF Tech. Report No. 57,ECMWF, Reading, UK, 72 pp.

Esbensen, S.K., and Y. Kushnir, 1981: The heat budget of the global ocean: An atlas based on estimates from surface marine observations. Climatic Research Institute, Report No. 29, Dept. Atmos. Sci., Oregon State Univ., Corvallis, OR.

Fouquart, Y., 1987: Radiative transfer in climate modeling. NATO Advanced Study Institute on Physically-Based Modeling and Simulation of Climate and Climatic Changes. Erice, Sicily, 11-23 May 1986. M.E. Schlesinger, Ed.,

Fouquart, Y., and B. Bonnel, 1980: Computations of solar heating of the Earth's atmosphere: A new parameterization. Beitr. Phys. Atmosph., 53, 35-62.

Fouquart, Y., B. Bonnel and V Ramaswamy, 1989: Intercomparing shortwave radiation codes for climate studies. Accepted for publication in J. Geophys. Res.

Geleyn, J.-F., and A. Hollingsworth, 1979: An economical analytical method for the computation of the interaction between scattering and line absorption of radiation. Beitr. Phys. Atmosph., 52, 1-16.

Geleyn, J.-F., A. Hense, and H.-J. Preuβ, 1982: A comparison of model-generated radiation fields with satellite measurements. Beitr. Phys. Atmosph., 55, 253-286.

Heckley, W.A., 1985: Systematic errors of the ECMWF operational forecasting model in tropical regions. Quart. J. Roy. Meteor. Soc., 111, 709-738.

Hollingsworth, A., K. Arpe, M. Tiedtke, M. Capaldo, and H. Savijärvi, 1980: The performance of a medium range forecast model in winter - Impact of physical parameterization. Mon. Wea. Rev., 108, 1736-1773.

Hollingsworth, A., A. Lorenc, M.S. Tracton, K. Arpe, G. Cats, S. Uppala, and P. Kallberg, 1985: The response of numerical weather prediction systems to FGGE level II-b data. Part I: Analyses. Quart. J. Roy. Meteor. Soc., 111, 1-66.

Hollingsworth, A., 1987: Objective analysis for numerical weather prediction, in: Short and Medium Range Numerical Weather Prediction. Collected papers presented at WMO/IUGG NWP Symposium, Tokyo, 4-8 August 1986, ed. by T. Matsuno, Special Volume of the J.Meteor.Soc.Japan, 11-59.

van Hoyt, D., 1976: The radiation and energy budgets of the Earth using both ground-based and satellite-derived values of total cloud cover. NOAA Tech. Report ERL 362-ARL4. U.S. Dept. of Commerce, Washington, D.C., 124 pp.

Jaeger, L., 1976: Monatskarten des Niederschlags für die Ganze Erde. Berichte des Deutschen Wetterdienstes, 139, 18.

Lönnberg, P., J. Pailleux, and A. Hollingsworth, 1986: The new analysis system. ECMWF Research Dept. Tech. Memo. No. 125, 21 pp., ECMWF, Reading, U.K.

Luther, F.M., R.G. Ellingson, Y. Fouquart, S. Fels, N.A. Scott, and W.J. Wiscombe, 1988: Intercomparison of radiation codes in climate models (ICRCCM): Longwave clear-sky results - a workshop summary. Bull. Amer. Meteor. Soc., 69, 40-48.

Morcrette, J.-J., 1989: Radiation and cloud radiative properties in the ECMWF operational weather forecast model. J. Geophys. Res., accepted for publication.

Morcrette, J.-J., and Y. Fouquart, 1985: On systematic errors in parametrized calculations of longwave radiation transfer. Quart. J. Roy. Meteor. Soc., 111, 565-585.

Morcrette, J.-J., and Y. Fouquart, 1986: The overlapping of cloud layers in shortwave radiation parameterizations. J. Atmos. Sci., 43, 321-328.

Morcrette, J.-J., and Y. Fouquart, 1988: Comparison of E.R.B.E. measurements with model-generated radiation fields. IRS'88: Current Problems in Atmospheric Radiation, J. Lenoble and J.-F. Geleyn, Eds., A. Deepak Publishing, Hampton, Va., 331-334.

Morcrette, J.-J., L. Smith, and Y. Fouquart, 1986: Pressure and temperature dependence of the absorption in longwave radiation parameterizations. Beitr. Phys. Atmosph., 59, 455-469.

NOAA, 1988: Climate Diagnostics Bulletin, August 1987. Available from NOAA/National Weather Service, National Meteorological Center, Climate Analysis Center, Washington, D.C.

Oberhuber, J.M., 1988: An Atlas based on the COADS dataset: The budget of heat, buoyancy and turbulent kinetic energy at the surface of the global ocean. Max-Planck-Institute for Meteorology Report No.15, Hamburg 13, F.R.G.

Ramanathan, V., E.J. Pitcher, R.C. Malone, and M.L. Blackmon, 1983: The response of a spectral general circulation model to refinements in radiative processes. J. Atmos. Sci., 40, 605-630.

Ramanathan, V., 1986: Atmospheric general circulation and its low frequency variance: Radiative influences. in: Short and Medium Range Numerical Weather Prediction. Collected papers presented at WMO/IUGG NWP Symposium, Tokyo, 4-8 August 1986, ed. by T. Matsuno, Special Volume of the J.Meteor.Soc.Japan, 11-59.

Ramanathan, V., 1987: The role of Earth Radiation Budget studies in climate and general circulation research. J. Geophys. Res., 92, 4075-4095.

Riehl, H., and J.S. Malkus, 1957: On the heat balance and maintenance of the circulation in the trades. Quart. J. Roy. Meteor. Soc., 83, 21-29.

Riehl, H., and J.J. Simpson, 1979: The heat balance of the equatorial trough zone: Revisited. Beitr. Phys. Atmosph., 52, 287-305.

Ritter, B., 1984: The impact of an alternative treatment of infrared radiation on the performance of the ECMWF forecast model. "IRS '84: Current problems in Atmospheric Radiation"., G. Fiocco, ed., A. Deepak Publ., Hampton, Va., 277-280.

Rothman, L.S., 1981: AFGL atmospheric absorption line parameters compilation: 1980 version. Appl. Opt., 20, 791-795.

Rothman, L.S.,R.R. Gamache, A. Barbe, A. Goldman, J.R. Gillis, L.R. Brown, R.A. Toth, J.-M. Flaud, and C. Camy-Peyret, 1983: AFGL atmospheric absorption line parameters compilation: 1982 edition. Appl. Opt. 15, 2247-2256.

Shaw, D.B., P. Lönnberg, A. Hollingsworth, and P. Undén, 1987: Data assimilation: The 1984/85 revisions of the ECMWF mass and wind analysis. Quart. J. Roy. Meteor. Soc., 113, 533-566.

Scott, N.A., and A. Chédin, 1981: A fast line-by-line method for atmospheric absorption computations: The Automatized Atmospheric Absorption Atlas. J. Appl. Meteor., 20, 802-812.

Simmons, A.J., D.M. Burridge, M. Jarraud, C. Girard, and W. Wergen, 1988: The ECMWF medium-range prediction models, Development of the numerical formulations and the impact of increased resolution. Meteor. Atmos. Phys., 40, 28-60.

Simmons, A.J., and M. Jarraud, 1984: The design and performance of the new ECMWF operational model. ECMWF Seminar on Numerical Methods for Weather Prediction. Vol. 2.

Simonot, J.-Y., and H. Le Treut, 1987: Surface heat fluxes from a numerical weather prediction system. Climate Dynamics, 2, 11-28.

Slingo, J.M., 1987: The development and verification of a cloud prediction scheme for the ECMWF model. Quart. J. Roy. Meteor. Soc., 113, 899-928.

Slingo, J.M., U.C. Mohanty, M. Tiedtke, and R.P. Pearce, 1988: Prediction of the 1979 Summer monsoon onset with modified parameterization schemes. Mon. Wea. Rev., 116, 328-346.

Slingo, A., and J.M. Slingo, 1988: The response of a general circulation model to cloud longwave radiative forcing. I: Introduction and initial experiments. Quart. J. Roy. Meteor. Soc., 114, 1027-1062.

Stephens, G.L., 1978: Radiative properties of extended water clouds. Part II: Parameterization schemes. J. Atmos. Sci., 35, 2111-2122.

Tiedtke, M., J.-F. Geleyn, A. Hollingsworth, and J.-F. Louis, 1979: ECMWF model: Parameterization of subgrid-scale processes. ECMWF Tech.Rep. No. 10., ECMWF, Reading, U.K.

Tiedtke, M., W.A. Heckley, and J. Slingo, 1988: Tropical forecasts at ECMWF: On the influence of physical parameterization on the mean structure of forecasts and analyses. Quart. J. Roy. Meteor. Soc., 114, 639-664.

Tiedtke, M., and M.J. Miller, 1988: Convection and its parameterization: Recent progress. ECMWF Research Dept. Tech. Memo. No. 147, 39 pp., ECMWF, Reading, U.K.

Trenberth, K.E., and J.G. Olson, 1988: ECMWF global analyses 1979-1986: Circulation statistics and data evaluation. NCAR Tech. Note NCAR/TN-300+STR, 94 pp.

Verstraete, M.V., and R.E. Dickinson, 1986: Modeling surface processes in atmospheric general circulation models. Annales Geophysicae, 4 B, 357-364.

Zdunkowski, W.G., G.J. Korb, and B.C. Nielsen, 1967: Prediction and maintenance of a radiation fog. U.S. Army Electronics Command Report. Contr. DAAB07-67-c-0049.

TECHNICAL REPORTS

No. 1 A case study of a ten day prediction.
K. Arpe, L. Bengtsson, A. Hollingsworth and Z. Janjic. September, 1976

No. 2 The effect of arithmetic precision on some meteorological integrations.
A.P.M. Baede, D. Dent and A. Hollingsworth. December, 1976

No. 3 Mixed-radix fourier transforms without reordering.
C. Temperton. February, 1977

No. 4 A model for medium range weather forecasts - adiabatic formulation.
D.M. Burridge and J. Haseler. March, 1977

No. 5 A study of some parameterisations of sub-grid processes in a baroclinic wave in a two dimensional model.
A. Hollingsworth. July, 1977

No. 6 The ECMWF analysis and data assimilation scheme: analysis of mass and wind field.
A. Lorenc, I. Rutherford and G. Larsen. December, 1977

No. 7 A ten-day high-resolution non-adiabatic spectral integration; a comparative study.
A.P.M. Baede and A.W. Hansen. October, 1977

No. 8 On the asymptotic behaviour of simple stochastic-dynamic systems.
A. Wiin-Nielsen. November, 1977

No. 9 On balance requirements as initial conditions.
A. Wiin-Nielsen. October, 1978

No. 10 ECMWF model parameterisation of sub-grid scale processes.
M. Tiedtke, J-F. Geleyn, A. Hollingsworth, and J-F. Louis. January, 1979

No. 11 Normal mode initialization for a multi-level grid-point model.
C. Temperton and D.L. Williamson. April, 1979

No. 12 Data assimilation experiments.
R. Seaman. October, 1978

No. 13 Comparison of medium range forecasts made with two parameterisation schemes.
A. Hollingsworth, K. Arpe, M. Tiedkte, M. Capaldo, H. Savijarvi, O. Akesson and J.A. Woods. October, 1978

No. 14 On initial conditions for non-hydrostatic models.
A.C. Wiin-Nielsen. November, 1978

No. 15 Adiabatic formulation and organization of ECMWF's spectral model.
A.P.M. Baede, M. Jarraud and U. Cubasch. November, 1979

No. 16 Model studies of a developing boundary layer over the ocean.
H. Okland. November, 1979

No. 17 The response of a global barotropic model to forcing by large scale orography.
J. Quiby. January 1980.

No. 18 Confidence limits for verification and energetic studies.
K. Arpe. May, 1980

No. 19 A low order barotropic model on the sphere with orographic and newtonian forcing.
E. Kallen. July, 1980

No. 20 A review of the normal mode initialization method.
Du Xing-yuan. August, 1980

No. 21 The adjoint equation technique applied to meteorological problems.
G. Kontarev. September, 1980

No. 22 The use of empirical methods for mesoscale pressure forecasts.
P. Bergthorsson. November, 1980

No. 23 Comparison of medium range weather forecasts made with models using spectral or finite difference techniques in the horizontal.
M. Jarraud, C. Girard and U. Cubasch. February, 1981

No. 24 On the average error of an ensemble of forecasts.
J. Derome. February, 1981

No. 25 On the atmospheric factors affecting the Levantine Sea.
E. Ozsoy. May, 1981

No. 26 Tropical influences on stationary wave motion in middle and high latitudes.
A.J. Simmons. August, 1981

No. 27 The energy budgets in North America, North Atlantic and Europe based on ECMWF analysis and forecasts.
H. Savijarvi. November, 1981

No. 28 An energy and angular momentum conserving finite-difference scheme, hybrid coordinates and medium range weather forecasts.
A.J. Simmons and R. Strüfing. November, 1981

No. 29 Orographic influences on Mediterranean lee cyclogenesis and European blocking in a global numerical model.
S. Tibaldi and A. Buzzi. February, 1982

No. 30 Review and re-assessment of ECNET - A private network with open architecture.
A. Haag, F. Konigshofer and P. Quoilin. May, 1982

No. 31 An investigation of the impact at middle and high latitudes of tropical forecast errors.
J. Haseler. August, 1982

No. 32 Short and medium range forecast differences between a spectral and grid point model. An extensive quasi-operational comparison. C. Girard and M. Jarraud
August, 1982

No. 33 Numerical simulations of a case of blocking: The effects of orography and land-sea contrast.
L.R. Ji and S. Tibaldi. September, 1982

No. 34 The impact of cloud track wind data on global analyses and medium range forecasts.
P. Kallberg, S. Uppala, N. Gustafsson and J. Pailleux. December, 1982

No. 35 Energy budget calculations at ECMWF. Part 1: Analyses 1980-81.
E. Oriol. December, 1982

No. 36 Operational verification of ECMWF forecast fields and results for 1980-1981.
R. Nieminen. February, 1983

No. 37 High resolution experiments with the ECMWF model: a case study.
L. Dell'Osso. September, 1983

No. 38 The response of the ECMWF global model to the El-Nino anomaly in extended range prediction experiments.
U. Cubasch. September, 1983

No. 39 On the parameterisation of vertical diffusion in large-scale atmospheric models.
M.J. Manton. December, 1983

No. 40 Spectral characteristics of the ECMWF objective analysis system.
R. Daley. December, 1983

No. 41 Systematic errors in the baroclinic waves of the ECMWF model.
E. Klinker and M. Capaldo. February, 1984

No. 42 On long stationary and transient atmospheric waves.
A.C. Wiin-Nielsen. August, 1984

No. 43 A new convective adjustment scheme.
A.K. Betts and M.J. Miller. October, 1984

No. 44 Numerical experiments on the simulation of the 1979 Asian summer monsoon.
U.C. Mohanty, R.P. Pearce and M. Tiedtke. October, 1984

No. 46 Cloud prediction in the ECMWF model.
J. Slingo and B. Ritter. January, 1985

No. 47 Impact of aircraft wind data on ECMWF analyses and forecasts during the FGGE period, 8-19 November, 1979.
A.P.M. Baede, P. Kallberg and S. Uppala. March, 1985

No. 48 A numerical case study of East Asian coastal cyclogenesis.
Shou-jun Chen and L. Dell'Osso. May, 1985

No. 49 A study of the predictability of the ECMWF operational forecast model in the tropics.
M. Kanamitsu. September, 1985

No. 50 On the development of orographic cyclones.
D. Radinovic. June, 1985

No. 51 Climatology and system error of rainfall forecasts at ECMWF.
F. Molteni and S. Tibaldi. October, 1985

No. 52 Impact of modified physical processes on the tropical simulation in the ECMWF model.
U.C. Mohanty, J.M. Slingo and M. Tiedtke. October, 1985

No. 53 The performance and systematic errors of the ECMWF tropical forecasts (1982-1984).
W.A. Heckley. November, 1985

No. 54 Finite element schemes for the vertical discretization of the ECMWF forecast model using linear elements.
D.M. Burridge, J. Steppeler and R. Strüfing. January, 1986

No. 55 Finite element schemes for the vertical discretization of the ECMWF forecast model using quadratic and cubic elements.
J. Steppeler. February, 1986

No. 56 Sensitivity of medium-range weather forecasts to the use of an envelope orography.
M. Jarraud, A.J. Simmons and M. Kanamitsu. September, 1986

No. 57 Zonal diagnostics of the ECMWF 1984-85 operational analyses and forecasts.
C. Brankovic. October, 1986

No. 58 An evaluation of the performance of the ECMWF operational forecasting system in analysing and forecasting tropical easterly wave disturbances. Part 1: Synoptic investigation.
R.J. Reed, A. Hollingsworth, W.A. Heckley and F. Delsol. September, 1986

No. 59 Diabatic nonlinear normal mode initialisation for a spectral model with a hybrid vertical coordinate.
W. Wergen. January, 1987

No. 60 An evaluation of the performance of the ECMWF operational forecasting system in analysing and forecasting tropical easterly wave disturbances. Part 2: Spectral investigation.
R.J. Reed, E. Klinker and A. Hollingsworth. January, 1987

No. 61 Empirical orothogonal function analysis in the zonal and eddy components of 500 mb height fields in the Northern extratropics.
F. Molteni. January, 1987

No. 62 Atmospheric effective angular momentum functions for 1986-1987.
G. Sakellarides. February 1989

No. 63 A verification study of the global WAM model. December 1987 - November 1988.
L. Zambresky. May 1989